Omega xxx (xxxx) xxx



Contents lists available at ScienceDirect

Omega

journal homepage: www.elsevier.com/locate/omega



Optimizing green infrastructure placement under precipitation uncertainty*

Masoud Barah^a, Anahita Khojandi^{b,*}, Xueping Li^b, Jon Hathaway^c, OluFemi Omitaomu^{b,d}

- ^a Department of Industrial Engineering and Management Sciences, Northwestern University, United States
- ^b Department of Industrial and Systems Engineering, The University of Tennessee, United States
- ^c Department of Civil and Environmental Engineering, The University of Tennessee, United States
- ^d Oak Ridge National Laboratory, United States

ARTICLE INFO

Article history: Received 21 December 2018 Accepted 8 January 2020 Available online xxx

Keywords: Green infrastructure Urban resilience Stochastic programming Chance constraint Climate change

ABSTRACT

Increased urbanization, infrastructure degradation, and climate change threaten to overwhelm stormwater systems across the nation, rendering them ineffective. Green Infrastructure (GI) practices are low cost, low regret strategies that can contribute to urban runoff management. However, questions remain as to how to best distribute GI practices through urban watersheds given precipitation uncertainty and the variable hydrological responses to them. We develop stochastic programming models to determine the optimal placement of GI practices across a set of candidate locations in a watershed to minimize the total expected runoff under medium-term precipitation uncertainties. Specifically, we first develop a two-stage stochastic programming model. Next, we reformulate this model using perturbed parameters to reduce the requisite computational time and extend it to multi-stage. In addition, we introduce constraints that allow for incorporating sub-catchment-level runoff reduction considerations. We account for hydrological connectivity in the watershed using an underlying acyclic connectivity graph of sub-catchments and incorporate various practical considerations into the models. In addition, we develop a systemic approach to downscale the existing daily precipitation projections into hourly units and efficiently estimate the corresponding hydrological responses. These advancements are brought together in a case study for an urban watershed in a mid-sized city in the U.S., where we perform sensitivity analyses, evaluate the importance of the considered constraints, and provide insights.

© 2020 Elsevier Ltd. All rights reserved.

1. Introduction

One of the most important factors threatening infrastructure in the U.S. is climate change. Climate change affects the frequency, intensity, spatial extent, duration as well as timing of extreme events [37]. Over the past decade, we have observed more frequent, intense and untimely events damaging infrastructure and impacting people and businesses (e.g., Hurricane Katrina, Superstorm Sandy). Thus, there are major concerns as to whether cities are protected against these projected increasing number of extreme weather events. To mitigate these effects, municipalities are beginning to seek opportunities to improve the resiliency of infrastructure through better urban planning and taking advantage of innovative solutions. This is extremely timely, as by the end of next decade, 60% of the world population will live in cities [73].

E-mail address: khojandi@utk.edu (A. Khojandi).

https://doi.org/10.1016/j.omega.2020.102196 0305-0483/© 2020 Elsevier Ltd. All rights reserved. Provision of scientifically-based methodologies for understanding and evaluating climate impacts will be critical to the development of adaptation strategies designed to avoid the increasing socioeconomic costs of severe weather-related damages to urban landscapes [60]. Despite this understanding, city managers are forced to make infrastructure decisions complicated by massive amounts of data and uncertainty. In a time when multiple, sometimes conflicting, climate projections exist, tools to distill these data into a usable format for such individuals are critical. Hence, city managers need a tool which addresses the complexity and uncertainty of climate projections to allow optimized choices for building resiliency into urban systems.

In the 2013 "Report Card" for American infrastructure, the nation's stormwater systems (in combination with wastewater) were awarded a D⁺, indicating the poor state of these critical components of the urban landscape. Exacerbating this need is the specter of climate change, leading us to the age of non-stationarity, where past trends of precipitation may no longer be relevant as a basis of design for civil infrastructure. Stormwater systems are particularly

 $^{^{\}scriptsize{\pm}}$ This manuscript was processed by AE Matsypura.

^{*} Corresponding author.

_

susceptible, as the size of pipes is selected based on how much stormwater needs to be conveyed for a given storm of interest or design storm applied to the watershed. As design storms are determined based on historical rainfall data, climate change threatens to overwhelm pipes that are in poor condition and undersized relative to changing weather patterns. Thus, climate change and the associated overwhelming of stormwater pipe systems is likely to cause increased flooding in urban watersheds, escalating the already present trend of flooding and flash flooding as (on average) the leading cause of weather-related fatalities in the U.S., beyond even hurricanes and tornadoes [45].

Replacing existing stormwater sewers with pipes of larger capacity would be prohibitively expensive and time consuming in many urban environments due to surrounding infrastructure and social conflicts. However, building resiliency into urban stormwater systems through the use of green infrastructure (GI) is an increasing trend nationwide. The 2014 Intergovernmental Panel on Climate Change (IPCC) has identified changes to urban drainage systems as a key adaption issue for North America and recommends consideration of lowregret strategies such as GI to reduce runoff while also providing co-benefits to freshwater provision, ecological processes, and freshwater fish populations [5,54]. The U.S. Environmental Protection Agency (EPA) is promoting GI as a means to enable communities to avoid costly water infrastructure replacement and repair by using vegetation and soil to manage rainwater where it falls, thereby reducing the burden on aging sewer pipes [19]. These systems act as localized storage centers, where stormwater can enter, be detained, then leave the system as evaporation, infiltration, or as runoff with diminished energy and volume. As such, GI has been deemed as a way to build better infrastructure as part of the National Academy of Engineering's Grand Challenge to restore and improve urban infrastructure.

In recent years, researchers have considered the impact of GI on urban flooding at the watershed scale [23,48]. Kim et al. [46] studied the impact of urban green spaces on reducing urban flood risk. As their case study, they considered a flooded area in Seoul, South Korea. They divided the case study area into four regions based on topographic and physical characteristics, and used logistic regression to determine how flooding probabilities change with respect to green space area. Based on their results, the probability of flooding could be reduced by over 50% depending on the location of green spaces and their types. In a related study, Liu et al. [49] developed a simulation model to determine the reduction of peak flow rate in flooding for an urban community in Beijing, China. They reported that an integrated GI configuration can reduce peak flow by 92.8-100%. Liu et al. [50] also investigated the impact of GI practice types and sizes on reducing urban flooding. They reported that expanding green spaces, concave green space, storage pond, and porous brick pavements are effective in reducing urban flooding. Using different sizes of these GI, they studied runoff reduction in 5-year recurrence storm and concluded that the proper GI combination together with appropriate GI sizing is necessary for urban stormwater runoff management. Thus, the properties of the GI and how it is configured in a given watershed have shown to be an important factor in literature for determining the effectiveness of these interventions [33,34].

Although the current body of work provides invaluable insights, to improve the resiliency of infrastructure, we need to modify our approach to infrastructure planning to account for future changes in climate. Accounting for extreme events does not necessarily translate into planning for the worst-case scenario; instead, it requires policymakers to allocate the budget and effort for future urban planning and maintenance actions by accounting for a wide range of factors *under uncertainty*. In our context, climate parameters, specifically future precipitation, are the main uncertainty. One important factor to consider when trying to optimize a measure of

interest under uncertainty, is that not only is knowledge about climate patterns limited and inherently stochastic, but there are multiple climate models that at times make inconsistent predictions. For example, Fig. 1 gives the projected annual precipitation, in inches, between 2018 and 2050 in the City of Knoxville, Tennessee, using 10 coupled general circulation models (CGCMs) [40]. As seen in the figure, there is significant difference between these 10 models in terms of annual precipitation levels, e.g., in year 2021, standard deviation of precipitation is 7.27 in. Hence, if placing GI practices in an urban watershed is performed under one projected scenario, it may fall extremely short of addressing the true stormwater management needs if another scenario is realized.

Stochastic programming has been used extensively for decision making under uncertainty, e.g., power systems [74], finance [47], and many engineering applications [52]. Specifically, this modelling approach has been extensively used in modeling facility location under uncertainty [66]. To the best of our knowledge, the use of this important methodology in environmental engineering applications has been limited, especially when it comes to placing GI practices in an urban environment under various uncertainties. Ramshani et al. [61] is perhaps one the few of such studies, and uses a stochastic programming model to optimally place PV panels and green roofs in a mid-sized city under climate change uncertainty to maximize the overall profit from energy generated and saved.

In this paper, we use stochastic programming to account for the uncertainty in future precipitation when placing GI practices in an urban watershed. Specifically, we first develop a two-stage stochastic programming model to determine the optimal placement of GI practices across a set of candidate locations in an urban watershed to minimize the total expected surface runoff under mediumterm precipitation uncertainty. Using statistical analysis on the performance of GI practices, we then develop a two-stage stochastic programming with perturbed parameters to produce alternative solutions to the problem of placing GI practices in an urban watershed Such approach results in a significant reduction in the requisite pre-processing and computational time. Next, we extend the formulation to multi-stage. Given the fact that some regions of the watershed may be of higher priority for runoff management, we then introduce constraints that allow for incorporating sub-catchment-level runoff reduction considerations. We conduct a case study for a watershed in the City of Knoxville, Tennessee, in which we calibrate the model using literature, historical precipitation data, future precipitation projections, watershed hydrological responses to precipitation and GI installations, and expert opinion. We provide the results under various levels of available budget, investigate their differences, conduct extensive sensitivity analyses, and provide insights.

No work has been identified in literature that addresses GI placement in an urban watershed under precipitation uncertainties. Perhaps the closet work is Loáiciga et al. [51]. Their objective was to minimize total construction cost such that volumetric water balance, stormwater volumes, and water-quality characteristics fell within an allowable range. However, this work does not account for the uncertainty in future precipitation projections.

The rest of the paper is organized as follows. First, we formulate the models in Section 2. Next, in Section 3, we calibrate the models for a watershed in a mid-size city in the U.S. In Section 4, we provide the computational results for our case study and draw insights. Finally, we provide a summary and additional insights in Section 5.

2. Model formulation

In this study, our goal is to minimize the expected total runoff volume over a medium-term planning horizon under future pre-

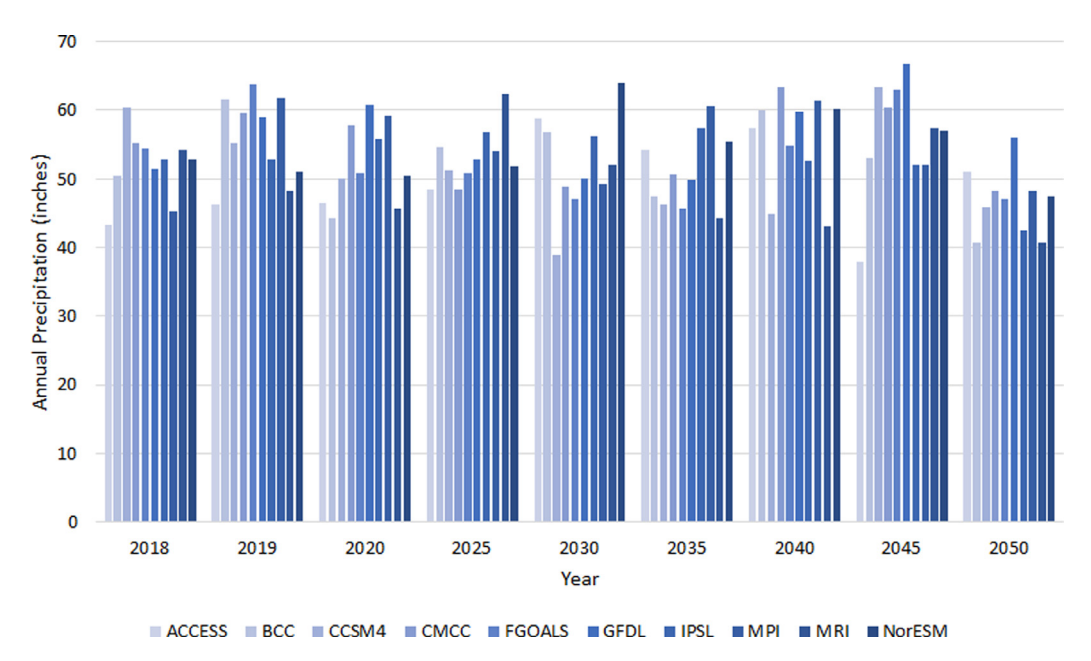


Fig. 1. Projected annual precipitation over the city of Knoxville, Tennessee, in inches, between 2018 and 2050 under 10 popular climate models.

cipitation uncertainty, given an available budget for investment. This is consistent with challenges currently facing city planners throughout the world.

Various types of GI differ in their expense, requirements for advanced planning, necessary land allocation, and their efficiency in reducing surface runoff following precipitation.

Accordingly, in this study, we consider two groups of GI practices, specifically, large-scale and small-scale GI practices. In our models, we allow for placing these GI practices under two settings, namely, 'restricted' and 'relaxed.' The former refers to the case where only GI practices of certain types can be placed in a given stage, whereas the latter relaxes this restriction, allowing all GI types to be placed in any stage. The former, although somewhat restrictive, provides practical benefits regarding investment planning and managing the efforts required for building the different types of GI practices.

First, in Section 2.1 we develop a base two-stage stochastic programming model under a restricted decision set, where large-scale and small-scale practices can only be placed in stages one and two, respectively, before and after a scenario is realized. Next, in Section 2.2, we re-cast the problem as a two-stage stochastic programming model that relies on perturbed parameters, under the same restricted decision set. We then relax the decision set assumption for this two-stage stochastic programming model and also extend this formulation to multi-stage, under the same relaxed decision set assumption. Finally, in Section 2.3, we introduce chance constraints that allow for incorporating sub-catchment-level runoff reduction considerations.

2.1. Stochastic programming model

In this section, we develop a two-stage stochastic programming model. The goal is determine the extent to which each subcatchment must be covered by each of the available types of GI, in the two stages, to minimize the expected total runoff over the planning horizon under precipitation uncertainty. For brevity, we refer to this model as 'stochastic model' in the remainder of the manuscript.

Let $V = \{1, 2, ..., |V|\}$ denote the set of sub-catchments within a watershed whose impervious areas are candidates for placing GI practices. For any given sub-catchment, let $G = \{1, 2, ..., |G|\}$ de-

note the set of all available types of GI practices. We assume that each GI practice may be installed in various levels within a given sub-catchment, e.g., to cover 5%, 7.5%, and 10% of the impervious area within any given sub-catchment with GI. Let $L = \{1, 2, ..., |L|\}$ denote the set of available levels of installation of GI practices within a given sub-catchment.

As discussed in Section 1, although CGCMs may be used to project future precipitation in a given region, the resulting projections from different models do not necessarily agree. Hence, the variability across these precipitation projections are the source of uncertainty in our model. Let T denote the length of the planning horizon in years and Ψ denote the finite set of projected precipitation time series for the watershed over the planning horizon T. We let $\psi \in \Psi$ denote a projected precipitation time series, corresponding to scenarios in the model, and π^{ψ} denote the realization probability of scenario $\psi \in \Psi$.

As discussed earlier in Section 2, we consider two groups of large- and small-scale GI practices in this study, where practices from the former and latter groups can be placed before and after a CGCM is realized. Let $T \leq T$ denote the year in which a precipitation scenario is realized. Hence, in the beginning of the planning horizon, before any scenarios are realized, we make firststage decisions. After T years into the planning horizon, we realize a certain CGCM, at which point we make second-stage decisions. Consequently, we continue with the realized CGCM for the rest of the planning horizon. Also, let G^I and G^{II} , where $G^I \cup G^{II} = G$, $G^{I} \cap G^{II} = \emptyset$, denote the set of possible types of GI practices available for placement at $t \leq \overline{T} - 1$ and $\overline{T} \leq t \leq T$, respectively. Consequently, let $x_{i,i,l}^t$ denote the first stage binary decision variable indicating whether or not a GI practice of type $j \in G^I \subset G$ in level *l* is placed within sub-catchment *i* in year $t \leq \overline{T} - 1$. Similarly, let $y_{i,i,l}^{\psi,t}$ denote the second stage binary decision variables indicating whether or not a GI practice of type $j \in G^{II} \subset G$ in level l is placed within sub-catchment i in $\overline{T} \le t \le T$. The decision variables assume the value 1 if the corresponding practice is installed, and the value 0, otherwise. Lastly, we let $\delta_{i,j,l}$ denote the corresponding area (in square feet) of GI practice type $j \in G$ installed in level $l \in L$, within sub-catchment $i \in V$. In this study, we assume only one type of GI can be placed in each sub-catchment, mainly due to the sizes of GI practices considered, compared to the sizes of the sub-catchments.

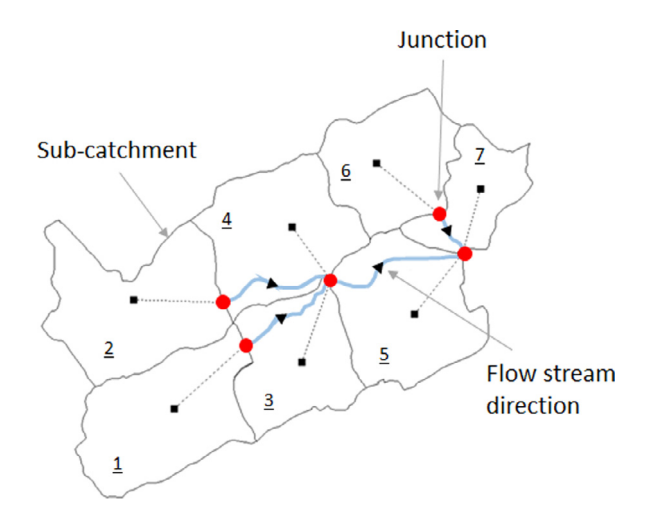


Fig. 2. A small portion of a watershed consisting of seven sub-catchments and its main stream.

Precipitation that is not infiltrated into the soil becomes surface runoff. We incorporate precipitation scenarios into our model by quantifying their impact on each sub-catchments' surface runoff reduction. Let $Q_i^{\psi,t}$ denote the total baseline surface runoff under scenario $\psi \in \Psi$ over sub-catchment $i \in V$ in year t when no GI practice is placed. Similarly, let $\hat{Q}_{i,j,l}^{\psi,t}$ denote the surface runoff captured by GI practice of type $j \in G$ installed in level $l \in L$ within subcatchment $i \in V$ under scenario $\psi \in \Psi$ in year t. Hence, clearly for any given $i \in V$, the difference between $Q_i^{\psi,t}$ and $\hat{Q}_{i,j,l}^{\psi,t}$ gives the total surface runoff in sub-catchment i over year t under scenario $\psi \in \Psi$ as a result of installing GI practices of type $j \in G$ in level $l \in L$ within the sub-catchment.

In this study, we assume that once a GI practice is constructed, it must be maintained annually to preserve its runoff reduction properties. Let $C_{i,j}^t$ denote the per square feet present total cost of placing GI practice of type j within sub-catchment i in year t. Also, let B denote the total available budget at the beginning of the planning horizon for placing GI practices.

A key goal to achieve in planning GI is connectivity as it provides additional resilience against urban runoff [25,29,38,44,55]. For instance, all else held constant, a series of connected GI practices is more effective in managing water quantity and quality than a set of disjoint GI practices that are surrounded by urban development [64]. This is mainly because runoff that flows from a sub-catchment to a downstream sub-catchment can be slowed or captured by GI practices before reaching downstream [38,44]. This impact is particularly pronounced in adjacent/neighboring sub-catchments with respect to watershed hydrology as the connected GI practices can further mitigate runoff resulting from 'directly connected impervious areas,' reducing runoff volumes, peak discharge, and base flow effects [57]. To that end, given that in this study we consider an urban watershed with many directly connected impervious areas, we impose certain connectivity constraints when placing GI practices to ensure that at least a minimum desired level of connectivity among GI practices is met.

Consider the following illustrative example that discusses the impact of various GI placements using a connected system of subcatchments. Fig. 2 illustrates a subset of a watershed consisting of seven sub-catchments and its main stream. Placing GI practices in any of the sub-catchments reduces the surface runoff in that subcatchment. Additionally, dependent on sub-catchments characteristics [24], placing a GI practice in an upstream sub-catchment, may further reduce the surface runoff in a downstream sub-catchment. Lastly, simultaneous placement of GI practices has the potential

to further mitigate the surface runoff, if the sub-catchments are 'hydrologically connected.' This is partly due to the fact that such placement can further disconnect the directly connected impervious areas within the sub-catchments. For instance, because subcatchments 3 and 5 are hydrologically connected, placing GI practices in sub-catchment 3 can potentially also reduce the amount of run-off over sub-catchment 5, even if no GI is placed on the latter sub-catchment. Furthermore, placing GI practices in both subcatchments 3 and 5 can potentially result in a larger reduction in surface runoff, compared to that obtained from placing the same type/level of GI practices in the two sub-catchments if they were not hydrologically connected.

We capture sub-catchment connectivity in a watershed using a directed acyclic graph. Specifically, let the directed acyclic graph $\mathbb{G}(V,A)$ denote the system of sub-catchments where V is the set of nodes in the graph, corresponding to the sub-catchments in the watershed, and A denotes the set of sub-catchment connectivity arcs, where there exists an arc $a_{i',i} \in A$ if and only if sub-catchments i', $i \in V$ are connected.

Consider a given pair of connected sub-catchments i' and i, $a_{i',i} \in A$. When accounting for surface run-off reduction over sub-catchment i due to a GI practice placed upstream, assuming large-scale GI practice installations only, three distinct cases must be considered: (a) a GI practice is placed within upstream sub-catchment i' in year t' after a GI is placed within downstream sub-catchment i in year t such that $0 \le t \le t' \le \overline{T} - 1$; (b) a GI is placed within upstream sub-catchment i' in year t' after a GI is placed within upstream sub-catchment i' in year t' such that $0 \le t' \le t \le \overline{T} - 1$; and (c) a GI is placed within upstream sub-catchment i' in year t' and no GI placed in downstream sub-catchment i' by the beginning of year \overline{T} , i.e., $0 \le t' \le \overline{T} - 1$.

To be able to account for the adjustment in surface runoff reduction due to GI installations in connected sub-catchments as described in cases (a)-(c), we introduce the runoff 'adjustment factor' $\beta_{i,j,l}^{i',j',l'}$ and the variable $z_{t,i,j,l}^{t',i',j',l'}$. Specifically, for any given pair of connected sub-catchments i' and i, where $a_{i',i} \in A$, we let $0 \le a_{i',i} \in A$. $\beta_{i,i,l}^{l',j',l'} \leq 1$ denote the runoff 'adjustment factor' over the downstream sub-catchment $i \in V$, when a GI practice of type $j' \in G^I$ in level $l' \in L$ is installed within upstream sub-catchment $i' \in V$ and no GI practice or a GI practice of type $j \in G^I$ in level $l \in L$ is installed within the downstream sub-catchment $i \in V$. We use j=0 to indicate that no GI is installed within a sub-catchment. In addition, we let $z_{t,i,j,l}^{t',i',j',l'}$ denote the binary variable indicating whether or not GI practices of types j', $j \in G^I$ in levels l', $l \in L$ are installed within sub-catchment i', $i \in V$ in years t', $t \leq \overline{T} - 1$, respectively. The variable assumes the value 1 if the corresponding practices are installed and equals 0, otherwise. In addition, we define $z_{t,i,0,l}^{t',i',j',l'} = 0$ for all t', i', j', l', t, i, and l, to account for cases when only the upstream sub-catchment is selected for installing large-scale GI practices. Note that a downstream sub-catchment can be hydrologically connected to more than one upstream subcatchment. We assume that the 'adjustments' over downstream sub-catchments are additive. Lastly, for completeness, we define $\hat{Q}_{i,0,l}^{\psi,t}=0$ for all ψ , t, i, and l to account for the case where no GI is installed in sub-catchment $i \in V$.

In addition to accounting for potential adjustments in runoff reduction as a result of hydrological connectivity, we require first stage decision variables to fulfill a certain connectivity constraint to ensure that the model provides at least a minimum desired level of connectivity among large-scale GI practices by the beginning of year \overline{T} . Specifically, we define GI connectivity as a 1-neighbor constraint on first stage decision variables, which prescribe large-scale GI practice installations. That is, a first stage GI practice can be installed in sub-catchment i if there exists at least one placed first

stage GI practice in one of the sub-catchments that are hydrologically connected to sub-catchment i. For simplicity of notation, in the remainder we use $x = [x_{i,j,l}^t]$, $z = [z_{t,i,j,l}^{t',i',j',l'}]$, $y = [y_{i,j,l}^{\psi,t}]$ to refer to the vectors of the corresponding variables. The notation is sum-

We let $\phi_S(x, z, y)$ denote the total expected surface runoff across the watershed $\mathbb{G}(V, A)$ over the planning horizon, T, under the decision variables x, z, and y for the stochastic model. Therefore, given the total available budget, B, the following model minimizes $\phi_S(x, z, y)$, i.e.,

marized in Appendix A.

$$\min_{\mathbf{x}, z, y} \phi_{S}(\mathbf{x}, z, y) \\
= \min_{\mathbf{x}, z, y} \sum_{\psi \in \Psi} \pi^{\psi} \cdot \left[\sum_{i \in V} \sum_{\{l \mid 0 \le t \le T\}} Q_{i}^{\psi, t} \right] \\
- \sum_{i \in V} \sum_{j \in G^{l}} \sum_{l \in L} \sum_{\{t \mid 0 \le t \le \overline{T}-1\}} \sum_{\{t' \mid t \le t' \le T\}} \widehat{Q}_{i, j, l}^{\psi, t'} \cdot \mathbf{x}_{i, j, l}^{t} \\
- \sum_{a_{i', i} \in A} \sum_{j \in G^{l} \cup \{0\}} \sum_{j' \in G^{l}} \sum_{i \in L} \sum_{l' \in L} \sum_{\{t \mid 0 \le t \le \overline{T}-1\}} \sum_{\{t' \mid 0 \le t' \le \overline{T}-1\}} \sum_{\{t' \mid 0 \le t' \le \overline{T}-1\}} \sum_{\{t'' \mid max\{t \cdot 1\}_{\{j \ne 0\}}, t'\} \le t'' \le T\} \\
\times \beta_{i, j, l}^{i', j', l'} \left(Q_{i}^{\psi, t''} \left(\mathbf{x}_{i', j', l'}^{t'} - \mathbf{z}_{t, i, j, l}^{t', i', j', l'} \right) + \widehat{Q}_{i, j, l}^{\psi, t''} \cdot \mathbf{z}_{t, i, j, l}^{t', i', j', l'} \right) \\
- \sum_{a_{i', i} \in A} \sum_{j \in G^{l} \cup \{0\}} \sum_{j' \in G^{l}} \sum_{i \in L} \sum_{l' \in L} \sum_{\{t \mid 0 \le t \le \overline{T}-1\}} \beta_{i, j, l}^{i', j', l'} \cdot Q_{i}^{\psi, t'} \cdot \mathbf{z}_{t, i, j, l}^{t', i', j', l'} \\
- \sum_{i \in V} \sum_{i \in I} \sum_{l \in L} \sum_{\{t \mid \overline{T}-t, z \in T\}} \sum_{\{t \mid l, t \mid \overline{T}-t, z \in T\}} \widehat{Q}_{i, j, l}^{\psi, t'} \cdot \mathbf{y}_{i, j, l}^{\psi, t'} \cdot \mathbf{y}_{i, j, l}^{\psi, t} \right], \tag{1}$$

$$\text{s.t.} \quad \sum_{i \in V} \sum_{j \in G^l} \sum_{l \in L} \sum_{\{t \mid 0 \leq t \leq \overline{T} - 1\}} C_{i,j}^t \cdot \delta_{i,j,l} \cdot X_{i,j,l}^t$$

$$+ \sum_{i \in V} \sum_{j \in C^{|I|}} \sum_{l \in L} \sum_{\{t \mid \overline{T} \le t \le T\}} C_{i,j}^t \cdot \delta_{i,j,l} \cdot y_{i,j,l}^{\psi,t} \le B,$$

$$\forall \psi \in \Psi,$$
 (2)

$$\begin{aligned} x_{i',j',l'}^{t'} + x_{i,j,l}^{t} &\leq z_{t,i,j,l}^{t',i',j',l'} + 1, & \forall i', i \in V, a_{i',i} \in A, \\ \forall j', j \in G^{l}, \forall l', l \in L, & 0 \leq t', t \leq \overline{T} - 1, \end{aligned} \tag{3}$$

$$x_{i,j,l}^{t} \geq \sum_{j' \in G^{l}} \sum_{l' \in L} \sum_{\{t' \mid 0 \leq t' \leq \overline{T} - 1\}} z_{t,i,j,l}^{t',i',j',l'}, \qquad \begin{cases} \forall i, i' \in V, a_{i',i} \in A, \\ \forall j \in G^{l}, \forall l \in L, \\ 0 \leq t \leq \overline{T} - 1, \end{cases}$$
(4)

$$x_{i',j',l'}^{t'} \geq \sum_{j \in G'} \sum_{l \in L} \sum_{\{t \mid 0 \leq t \leq \overline{T}-1\}} z_{t,i,j,l}^{t',i',j',l'}, \qquad \begin{array}{l} \forall i,i' \in V, a_{i',i} \in A, \\ \forall j' \in G^l, \forall l' \in L, \\ 0 \leq t' \leq \overline{T}-1, \end{array} \tag{5}$$

$$\begin{split} z^{t',i',j',l'}_{t,i,j,l} &= 0, \\ z^{t',i',j',l'}_{t,i,j,l} &= 0, \\ 0 &\leq t,t' \leq \overline{T} - 1, \end{split}$$

$$\sum_{j \in G'} \sum_{l \in L} \sum_{\{t \mid 0 \le t \le \overline{T} - 1\}} x_{i,j,l}^{t} \le \sum_{a_{i',i} \in A} \sum_{j \in G'} \sum_{l \in L} \sum_{\{t \mid 0 \le t \le \overline{T} - 1\}} x_{i',j,l}^{t},$$

$$\forall i \in V,$$
(6)

$$\sum_{j \in G^{l}} \sum_{l \in L} \sum_{\{t \mid 0 \le t \le \overline{T} - 1\}} x_{i,j,l}^{t} + \sum_{j \in G^{ll}} \sum_{l \in L} \sum_{\{t \mid \overline{T} \le t \le T\}} y_{i,j,l}^{\psi,t} \le 1,
\forall i \in V, \psi \in \Psi,$$
(8)

$$\begin{array}{ll} \forall i', i \in V, a_{i',i} \in A, \\ \forall j', j \in G^{l}, \forall j'' \in G^{ll}, \\ x_{i,j,l}^{t}, y_{i,j'',l}^{t',t'}, z_{t,i,j,l}^{t',i',j',l'} \in \{0,1\}, \\ x_{i,j,l}^{t}, y_{i,j'',l}^{t',t'}, z_{t,i,j,l}^{t',i',j',l'} \in \{0,1\}, \\ 0 \leq t, t' \leq \overline{T} - 1, \\ \overline{T} \leq t'' \leq T. \end{array} \tag{9}$$

The objective function (1) minimizes the total expected surface runoff across the sub-catchments within the watershed over the planning horizon. The first term in (1) captures the total baseline runoff. The second term in (1) presents the reduction in surface runoff over the sub-catchments as a result of first stage GI installations within the sub-catchments. The third and forth terms in (1) address the adjustment in surface runoff reduction due to GI installations in connected sub-catchments (see Appendix B for more details). Finally, the last term in (1) presents the reduction in surface runoff over the sub-catchments as a result of second-stage GI installations within the sub-catchments.

Constraint (2) enforces budget limitations for placing GI practices. Constraints (3)–(6) establish the relationship between variables x and z and enforces the latter to assume the value one when large-scale GI practices are installed within two connected sub-catchments, and to assume the value zero, otherwise. Constraint (7) ensures the 1-neighbor connectivity among first-stage GI practices. Constraint (8) assures that at most one GI practice is installed in any given sub-catchment throughout the planning horizon. Finally, constraint (9) enforces binary restrictions on the decision variables. Let Ω denote the feasible set of the problem, i.e., $\Omega = \{\chi = (x,z,y)|(2)-(9)\}$. Accordingly, we let $\chi_S^* \in \Omega$ denote the optimal solution to the stochastic model, i.e., $\phi_S(\chi_S^*) \leq \phi_S(\chi)$ for all $\chi \in \Omega$.

2.2. Stochastic programming model with perturbed parameters

In this section, we first use the notation introduced in Section 2.1 to re-cast the problem as a two-stage stochastic programming model with perturbed baseline runoff and runoff capturing parameters. We then extend the model to multi-stage (particularly accounting for three stages). For brevity, we refer to these models as 'conservative-stochastic models' in the remainder of the manuscript.

We first present a two-stage conservative-stochastic programming model. Similar to the previous formulation, the model prescribes the extent to which each sub-catchment must be covered by each type of GI practice in the two stages. Different from the previous formulation in which the baseline surface runoff volume, $\mathbf{Q}_i^{\psi,t}$, and surface runoff volume captured by a GI practice, $\hat{\mathbf{Q}}_{i,j,l}^{\psi,t}$, were assumed to be readily known, in this formulation we assume there is uncertainty in calculating these runoff volumes.

Specifically, we redefine $Q_i^{\psi,t}$ to denote the *average* baseline surface runoff volume within sub-catchment $i \in V$ under scenario $\psi \in \Psi$ in year t, and let $2q_i^{\psi,t}(\alpha)$ denote the width of the $100(1-\alpha)\%$ confidence interval (CI) for the corresponding average baseline surface runoff volume. Similarly, we redefine $\hat{Q}_{i,j,l}^{\psi,t}$ to denote the *average* surface runoff volume captured by GI practice of type $j \in G$ installed in level $l \in L$ within sub-catchment $i \in V$ under scenario $\psi \in \Psi$ in year t, and let $2\hat{q}_{i,j,l}^{\psi,t}(\alpha)$ denote the width of the $100(1-\alpha)\%$ CI for the corresponding average surface runoff volume captured by the GI practice. Consequently, $[Q_i^{\psi,t} - q_i^{\psi,t}(\alpha), Q_i^{\psi,t} + q_i^{\psi,t}(\alpha)]$ and $[\hat{Q}_{i,j,l}^{\psi,t} - \hat{q}_{i,j,l}^{\psi,t}(\alpha), \hat{Q}_{i,l,j}^{\psi,t} + \hat{q}_{i,j,l}^{\psi,t}(\alpha)]$ give the corresponding $100(1-\alpha)\%$ CI for the average baseline surface runoff volume and runoff volume captured, respectively. Accordingly, the average baseline runoff volume and runoff volume captured by the given GI practice within sub-catchment $i \in V$ under scenario $\psi \in \Psi$ in year t are no worse than the CI upper

c

bound $Q_i^{\psi,t} + q_i^{\psi,t}(\alpha)$ and the CI lower bound $\hat{Q}_{i,j,l}^{\psi,t} - \hat{q}_{i,j,l}^{\psi,t}(\alpha)$, respectively, $100(1-\alpha)\%$ of the time.

Finally, consistent with Soyster's method [67], in our objective function of the conservative-stochastic model, compared with that of the stochastic model in Eq. (1), we use the $100(1-\alpha)\%$ CI upper bound and lower bounds of the estimated values for $Q_i^{\psi,t}$ and $\hat{Q}_{i,j,l}^{\psi,t}$ to take a conservative view. Accordingly, we let $\phi_{R_\alpha}(x,z,y)$ denote the total expected surface runoff volume across the watershed $\mathbb{G}(V,A)$ over the planning horizon, T, under the decision variables x, z, and y for the conservative-stochastic model. Therefore, given the total available budget, B, the following model minimizes $\phi_{R_\alpha(x,z,y)}$. Note that analogous to the stochastic model, we let $\chi_R^* \in \Omega$ denote the optimal solution to the conservative-stochastic model.

$$\min_{\mathbf{x},z,y} \phi_{\mathcal{R}_{\alpha}}(\mathbf{x},z,y) \\
= \min_{\mathbf{x},z,y} \sum_{\psi \in \Psi} \pi^{\psi} \cdot \left[\sum_{i \in V} \sum_{t \mid 0 \le t \le T} Q_{i}^{\psi,t} + q_{i}^{\psi,t}(\alpha) \right] \\
- \sum_{i \in V} \sum_{j \in G^{I}} \sum_{l \in L} \sum_{\{t \mid 0 \le t \le \overline{I}-1\}} \sum_{\{t' \mid t \le t' \le T\}} \left(\hat{Q}_{i,j,l}^{\psi,t'} - \hat{q}_{i,j,l}^{\psi,t'}(\alpha) \right) \cdot x_{i,j,l}^{t} \\
- \sum_{a_{i',i} \in A} \sum_{j \in G^{I} \cup \{0\}} \sum_{j' \in G^{I}} \sum_{l \in L} \sum_{l' \in L} \sum_{\{t \mid 0 \le t \le \overline{I}-1\}} \sum_{\{t' \mid 0 \le t' \le \overline{I}-1\}} \sum_{\{t'' \mid max\{t \cdot 1\}_{\{j \ne 0\}}, t'\} \le t'' \le T\}} \\
\times \beta_{i,j,l}^{i',j',l'} \left(\left(Q_{i}^{\psi,t''} - q_{i}^{\psi,t''}(\alpha) \right) \cdot z_{t,i,j,l}^{t',i',j',l'} - z_{t,i,j,l}^{t',i',j',l'} \right) \\
+ \left(\hat{Q}_{i,j,l}^{\psi,t''} - \hat{q}_{i,j,l}^{\psi,t''}(\alpha) \right) \cdot z_{t,i,j,l}^{t',i',j',l'} \right) \\
- \sum_{a_{i',i} \in A} \sum_{j \in G^{I} \cup \{0\}} \sum_{j' \in G^{I}} \sum_{l \in L} \sum_{l \in L} \sum_{t' \in L} \sum_{\{t \mid 0 \le t \le \overline{I}-1\}} \sum_{\{t' \mid 0 \le t' \le t-1\}} \sum_{\{t'' \mid t' \le t'' \le t-1\}} \sum_{\{t'' \mid t' \le t'' \le T-1\}} \sum_{t'' \mid t'' \mid t'''} \sum_{j' \in D^{I}} \sum_{l \in L} \sum_{t \mid \overline{I} \le t \le T} \sum_{\{t' \mid t \le t' \le T\}} \left(\hat{Q}_{i,j,l}^{\psi,t'} - \hat{q}_{i,j,l}^{\psi,t'}(\alpha) \right) \cdot y_{i,j,l}^{\psi,t} \right],$$
s.t. $\chi = (x, z, y) \in \Omega$. (10)

Although the objective function in the conservative-stochastic model may seem overly conservative compared with the one in the stochastic model, that only accounts for average volumes, we believe such a model is practical in our context. Note that the intensity of precipitation, i.e., the amount of precipitation in a period of time (especially for short periods, e.g., 24 hours) is an important predictor of, and is negatively correlated with, GI practice performance [22]. Assuming that the precipitation intensity is relatively similar across all sub-catchments in a relatively small watershed, when intense precipitation occurs, the performance of all GI practices are expected to get worse. This means that the resulting runoff across all sub-catchments would increase accordingly and, in turn, in Eq. (1) all coefficients pertaining to baseline surface runoff volume, $Q_i^{\psi,t}$, and surface runoff volume captured by GI practices, $\hat{Q}_{i,j,l}^{\psi,t}$, must be adjusted.

Next, we extend the problem formulation to multi-stage conservative-stochastic programming (particularly accounting for three stages). Recall that in the two-stage case, in the beginning of the planning horizon, before any scenarios are realized, we make first-stage decisions. After \overline{T} years into the planning horizon, we realize a certain CGCM, at which point we make second-stage decisions. In contrast, in the three-stage case, we expand each node of the second-stage decision tree with scenarios that pertain to all CGCMs. That is, in the second stage, instead of realizing one single CGCM for the rest of the planning horizon, we may continue with any of the CGCMs until stage three. Given the fact that we have realized a CGCM at the second stage, we assume that this CGCM

is more likely to occur between this stage and the third stage. Finally, we realize a certain CGCM at the third stage, at which point we make third-stage decisions. Consequently, we continue with the realized CGCM for the rest of the planning horizon. The complete discussion on the model formulation of the multi-stage stochastic programming model with perturbed parameters is included in Appendix C.

2.3. Incorporating sub-catchment-level runoff reduction considerations

Note that the models developed so far aim to minimize the expected total runoff volume under future precipitation uncertainty, without any requirements for runoff reduction across individual sub-catchments. However, to increase resilience against precipitation uncertainty, it is important to be able to minimize the expected total runoff volume across the entire watershed, while accounting for some level of confidence in runoff mitigation in certain (or all) sub-catchments. For instance, such measures may be of particular interest in dense residential regions where higher runoff may result in significant water quality problems. As such, next we introduce a chance constraint that ensures the GI practices are placed across the watershed such that some level of confidence in the degree of runoff volume captured in a given subcatchment is achieved. Such constraints enable the prioritization of sub-catchments when placing GI practices.

First, we let the random variable $\xi_i^{\psi,t}$ denote the expected baseline surface runoff volume over sub-catchment i under scenario ψ in year t, such that $\mathbb{E}[\xi_i^{\psi,t}] = Q_i^{\psi,t}$. Similarly, we let the random variable $\hat{\xi}_{i,j,l}^{\psi,t}$ denote the expected runoff volume captured by GI practice of type j installed in level l within sub-catchment i under scenario ψ in year t, such that $\mathbb{E}[\hat{\xi}_{i,j,l}^{\psi,t}] = \hat{Q}_{i,j,l}^{\psi,t}$. Let γ_i^t denote a desired minimum threshold for the proportion of runoff volume captured due to placing GI practices in sub-catchment i in year t. In addition, we let $1-\epsilon$ denote the desired confidence level for satisfying this minimum threshold. Therefore, for any given sub-catchment i, we have

$$\Pr\left(\frac{\sum_{j\in G}\sum_{l\in L}\hat{\xi}_{i,l,j}^{\psi,t}\left(x_{i,j,l}^{t}+y_{i,l,j}^{\psi,t}\right)}{\xi_{i}^{\psi,t}}\geq \gamma_{i}^{t}\right)\geq 1-\epsilon \quad \forall \psi\in \Psi, 0\leq t\leq T.$$

$$\tag{11}$$

Note that for simplicity in notation, we present the constraint when assuming $G^I = G^{II} = G$. However, similar constraints may be written when $G^I \neq G^{II}$.

Next, suppose $\xi_i^{\psi,t}$ and $\hat{\xi}_{i,j,l}^{\psi,t}$ are normally distributed. Note that their means equal to $Q_i^{\psi,t}$ and $\hat{Q}_{i,j,l}^{\psi,t}$, respectively, and their standard deviations can be respectively computed from the $(1-\alpha)$ % CIs defined in Section 2.2, namely, $[Q_i^{\psi,t}-q_i^{\psi,t}(\alpha),Q_i^{\psi,t}+q_i^{\psi,t}(\alpha)]$ and $[\hat{Q}_{i,j,l}^{\psi,t}-\hat{q}_{i,j,l}^{\psi,t}(\alpha),\hat{Q}_{i,l,j}^{\psi,t}+\hat{q}_{i,j,l}^{\psi,t}(\alpha)]$. That is, for $\alpha=0.05$, the $2q_i^{\psi,t}(0.05)$ and $2\hat{q}_{i,j,l}^{\psi,t}(0.05)$ are approximately equal to four times the standard deviations of $\xi_i^{\psi,t}$ and $\hat{\xi}_{i,j,l}^{\psi,t}$, respectively. Hence, considering $\alpha=0.05$, we let $\xi_i^{\psi,t}\sim\mathcal{N}(Q_i^{\psi,t},(q_i^{\psi,t}(0.05))^2/4)$ and $\hat{\xi}_{i,j,l}^{\psi,t}\sim\mathcal{N}(\hat{Q}_{i,j,l}^{\psi,t},(\hat{q}_{i,j,l}^{\psi,t}(0.05))^2/4)$. Also, we let $\sum_{i,j,l}^{\psi,t}$ denote the covariance of the random variables $\xi_i^{\psi,t}$ and $\hat{\xi}_{i,j,l}^{\psi,t}$. Let $\zeta_i^{\psi,t}=\sum_{j\in G}\sum_{l\in L}\hat{\xi}_{i,l,j}^{\psi,t}(x_{i,j,l}^t+y_{i,l,j}^{\psi,t})-\gamma_i^t\xi_i^{\psi,t}$. Hence, for fixed x and y, we have

$$\zeta_i^{\psi,t} \sim \mathcal{N}\left(\overline{\zeta}_i^{\psi,t} = \sum_{i \in I} \sum_{l \in I} \hat{Q}_{i,l,j}^{\psi,t} \left(x_{i,j,l}^t + y_{i,l,j}^{\psi,t}\right) - \gamma_i^t Q_i^{\psi,t},\right)$$

$$\begin{split} \sigma_{\zeta_{i}^{\psi,t}}^{2} &= \sum_{j \in G} \sum_{l \in L} \frac{(\hat{q}_{i,j,l}^{\psi,t}(0.05))^{2}}{4} \bigg(x_{i,j,l}^{t} + y_{i,l,j}^{\psi,t} \bigg)^{2} \\ &+ (\gamma_{i}^{t})^{2} \frac{(q_{i}^{\psi,t}(0.05))^{2}}{4} - \sum_{i \in G} \sum_{l \in L} 2 \gamma_{i}^{t} \Sigma_{i,j,l}^{\psi,t} \bigg(x_{i,j,l}^{t} + y_{i,l,j}^{\psi,t} \bigg) \bigg). \end{split}$$

Note that according to constraint (8) and binary condition on variables, $(x + y)^2 = (x + y)$. Also, due to the constraint, the covariance between $\hat{\xi}_{i,l,j}^{\psi,t}$ variables (for all j and l) is zero. Hence, Eq. (11) simplifies as follows:

$$\Pr\left(\zeta_i^{\psi,t} \geq 0\right) = \Pr\left(u \geq -\frac{\overline{\zeta}_i^{\psi,t}}{\sigma_{\zeta_i^{\psi,t}}}\right) \geq 1 - \epsilon \Longleftrightarrow -\frac{\overline{\zeta}_i^{\psi,t}}{\sigma_{\zeta_i^{\psi,t}}} \leq \Phi^{-1}(\epsilon).$$

Finally, by replacing $\overline{\zeta}_i^{\psi,t}$ and $\sigma_{\zeta_i^{\psi,t}}$ in the above equation and squaring the sides, chance constraint (11) turns into the following

$$\begin{split} &\sum_{j \in G} \sum_{l \in L} \left(\hat{Q}_{i,l,j}^{\psi,t} \right)^{2} \left(x_{i,j,l}^{t} + y_{i,l,j}^{\psi,t} \right) \\ &- 2 \gamma_{i}^{t} Q_{i}^{\psi,t} \left(\sum_{j \in G} \sum_{l \in L} \hat{Q}_{i,l,j}^{\psi,t} \left(x_{i,j,l}^{t} + y_{i,l,j}^{\psi,t} \right) \right) \\ &\times \left(\gamma_{i}^{t} \right)^{2} \left(Q_{i}^{\psi,t} \right)^{2} \\ &+ \left(\sum_{j \in G} \sum_{l \in L} \frac{\left(\hat{q}_{i,j,l}^{\psi,t} (0.05) \right)^{2}}{4} \left(x_{i,j,l}^{t} + y_{i,l,j}^{\psi,t} \right) \left(\gamma_{i}^{t} \right)^{2} \frac{\left(q_{i}^{\psi,t} (0.05) \right)^{2}}{4} \right. \\ &+ \sum_{j \in G} \sum_{l \in L} 2 \gamma_{i}^{t} \sum_{i,j,l}^{\psi,t} \left(x_{i,j,l}^{t} + y_{i,l,j}^{\psi,t} \right) \left(\Phi^{-1}(\epsilon) \right)^{2} & \leq 0, \quad \forall i \in V, \\ & 0 \leq t \leq T - 1 \end{split}$$

3. Model calibration

In this section, we calibrate the mathematical models presented in Section 2 using literature, historical data, precipitation projections, and expert opinion for an urban watershed of a mid-sized city in the U.S. First, in Section 3.1 we calibrate the parameters associated with GI practices. Next, in Section 3.2 we discuss the preprocessing performed on precipitation projections to convert them into the requisite format. Finally, in Section 3.3 we describe the hydrological simulations performed to characterize the surface runoff resulting from precipitation projections in the sub-catchments, under potential GI placements.

3.1. GI Practices

The performance of a GI practice can be described as the volume of surface runoff that the practice can infiltrate on an hourly basis [65]. The performance of GI practices depend on an array of factors including design specifications (such as surface storage volume, media storage, and media composition and depth, etc.) and climate patterns (such as precipitation event intensity and duration, etc.) [26,69]. In addition, maintenance activities must be performed for GI practices to continue their performance [6].

GI types, G, and GI installation levels, L. In this study, we consider two common types of GI practices, namely, bioretention and rain garden [30], hence |G| = 2. The former is typically installed in relatively large, commercial scales and is held to a higher design standard, whereas the latter is a smaller system with lower design standards and is placed in residential lots [9]. In two-stage stochastic models, under the restricted decision set assumption, we let the bioretentions and rain gardens be placed in the first and second stages, respectively. Hence, in these models we use $|G^I| = 1$ and

 $|G^{II}| = 1$. Under relaxed decision sets, however, we allow bioretentions and rain gardens to be placed in any of the decision stages, i.e., |G| = 2 in all stages.

The amount of surface runoff reduction by GI practices in any given sub-catchment of a watershed is closely related to the surface area that they cover from the corresponding sub-catchment [63]. We account for three levels of installation for each of the two GI practice types considered, i.e., |L| = 3. National Association of City Transportation Officials (NACTO) [13] recommends using the effective impervious surface area in the drainage region (subcatchments) as a key design factor when sizing bioretentions [14]. To that end, and due to the larger scale of bioretention installation, in this study we allow bioretentions to cover 5%, 7.5%, and 10% of the impervious area of each sub-catchment. Given the size of a sub-catchment, these ratios can be translated into square feet to obtain the corresponding values of $\delta_{i,j,l}$. For rain gardens, due to their residential-scale implementation, we allocate the total areas of 2500, 5000, and 7500 square feet for placing the GI practices within each sub-catchment. Finally, note that for the general attributes of the two types of GI practices considered, e.g., minimum media depth, ponding depth, media permeability, we use the stormwater training manuals from State of Tennessee Department of Environment & Conservation [17].

GI costs, $C_{i,j}^t$. The total cost of placing GI practices includes construction and maintenance costs. Let $c_{i,j}^t$ and $c_{i,j}^t$ denote the per square feet construction and annual maintenance costs of a GI practice of type i in sub-catchment i in year $t \leq T$, respectively. We assume the maintenance cost incurs annually starting from the vear of construction and is subject to an annual increase with the average annual inflation rate r. Hence, the present value at time zero of the total per square feet cost of placing GI practice of type *i* in sub-catchment *i* at time *t* is given by

$$C_{i,j}^{t} = \frac{1}{(1+r)^{t}} \cdot \left(c_{i,j}^{t} + \frac{1-r^{T-t}}{1-r} \cdot c_{i,j}^{t}\right).$$

We use the inflation-adjusted EPA Opti-Tool [32] and the University of Texas A&M's AGRILIFE Report [35] to obtain the per square feet construction cost of bioretentions and rain gardens, respectively. For instance, the reported per square feet construction cost of bioretentions was \$15.46 in 2016, and that of rain gardens was \$6.00 in 2012. To estimate the corresponding costs during the planning horizon, we adjust the values using the U.S. Labor Department's Consumer Price Index (CPI) inflation calculator [72]. We do not consider land cost in this study as we assume all GI practices are placed on public land or on land parcels offered by private property owners. Based on published reports [68], the annual GI maintenance cost ranges between 3% - 6% of its construction cost. Let ρ denote the ratio of maintenance cost to construction cost, i.e., $\rho = c_{i,j}^t/c_{i,j}^t$. In this study, we set $\rho = 3\%$. Lastly, we use the average annual inflation rate r = 1.86%, which equals the average annual U.S. inflation rate over the period 2007–2017 [18].

3.2. Pre-processing of precipitation projections

As discussed in Section 1, CGCMs project future precipitation, which are next fed to hydrological simulators to calculate the resulting surface runoff, at various degrees of GI installation. In this study, we use precipitation projections for the City of Knoxville produced by ten CGCMs (see Table D.1 in Appendix D for more detail.) Note that using CGCMs to produce projections are computationally expensive and hence, the projections are usually only produced in daily units. Let $\hat{\psi} \in \hat{\Psi}$ denote a daily precipitation projection time series produced by one of the ten CGCMs. To accurately capture the GI response to precipitation, more granular data, i.e., hourly precipitation projections, are required due to quick trans-

Please cite this article as: M. Barah, A. Khojandi and X. Li et al., Optimizing green infrastructure placement under precipitation uncer-

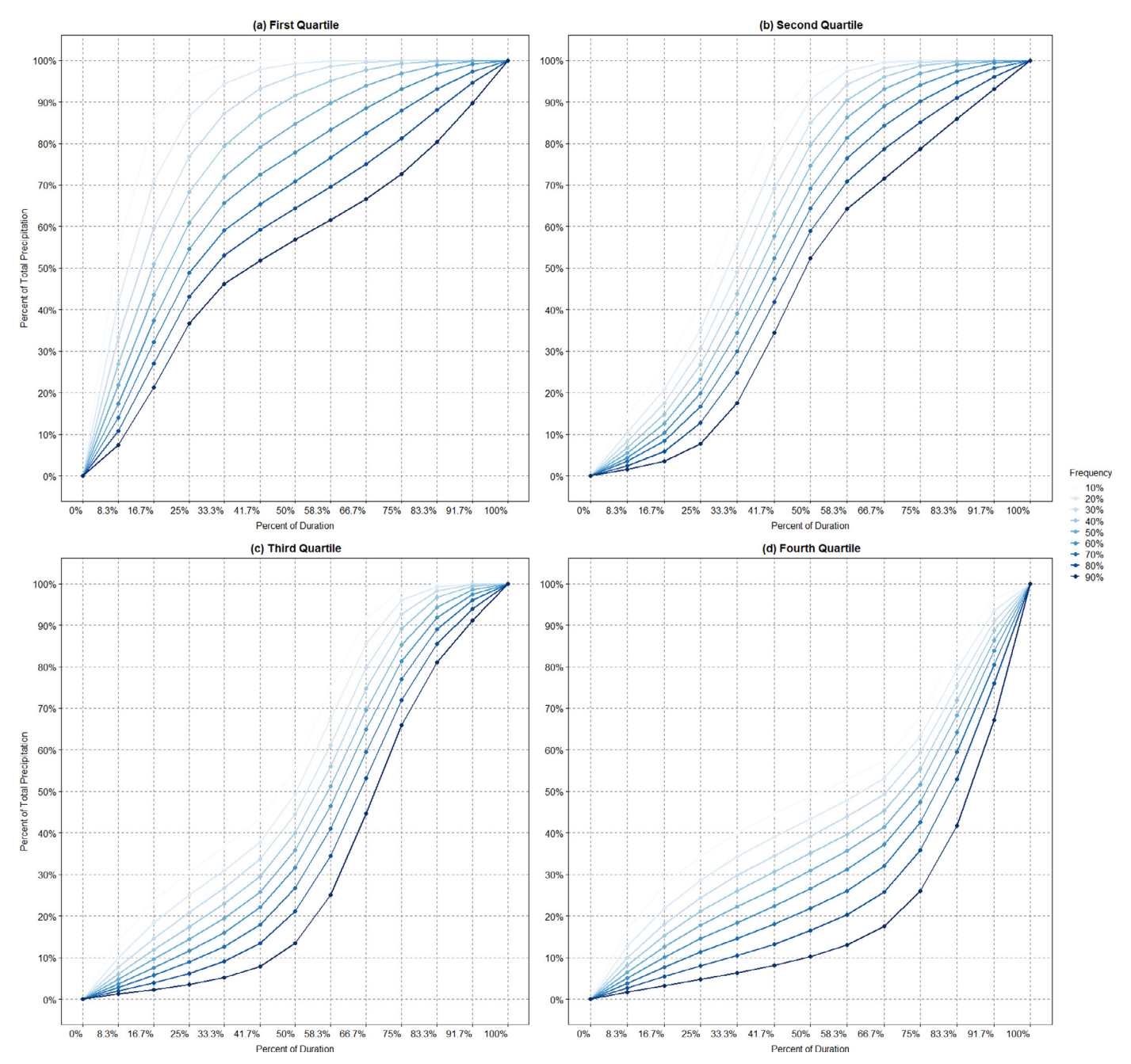


Fig. 3. Quartile-based Temporal distributions of daily precipitation, adapted from [20].

port of runoff in urban watersheds. Therefore, the daily precipitation projections must be converted into hourly precipitation projections, denoted by $\psi \in \Psi$, before they can be fed into hydrological simulators to calculate corresponding amounts of surface runoff.

Note that hourly precipitation projections can be uniquely aggregated to produce daily precipitation projections; however, the reverse is not true. In this section, we present an approach for preprocessing daily precipitation projections to generate one of the many likely hourly precipitation projections. Specifically, we use quartile-based and seasonal-based temporal distributions [20] to convert a daily precipitation time series into an hourly precipitation time series. Temporal distributions of precipitation summarize the historical cumulative percentages of precipitation up to any

point during a precipitation event and provide the proportion of time that the pattern was observed.

Fig. 3 presents the quartile-based distributions of 24-hour precipitation of Ohio river basin (including the City of Knoxville), adopted from Precipitation-Frequency Atlas of the United States [20]. Specifically, Fig. 3(a)–(d) present the cumulative probability plots of temporal distributions, where the highest percentage of precipitation during the 24-hour period occurred in the first-fourth quarters of the day, respectively. For instance, Fig. 3(a) presents the temporal distributions, where the highest amount of daily precipitation occurred during the first quarter of the day. The nine cumulative distributions in each panel present the nine general patterns according to which the corresponding amount of precipitation was accumulated. The shades of the distributions present the percentage of time that the particular pattern

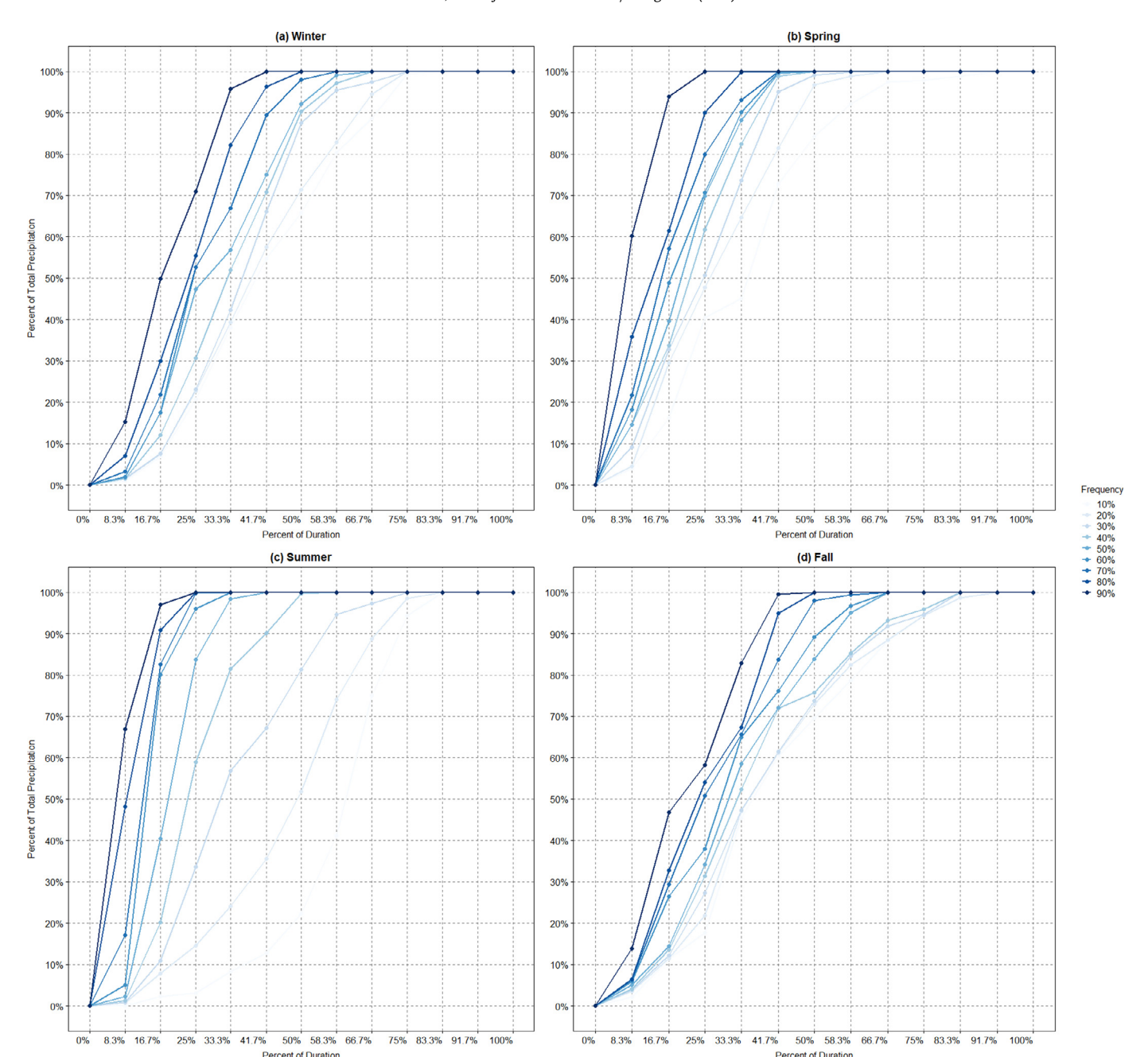


Fig. 4. Seasonal-based temporal distributions of daily precipitation.

was observed. For instance, given that the highest percentage of daily precipitation occurred in the first quantile (Fig. 3(a)), in 10% of the cases, 55.1% of total daily precipitation occurred during the first 8.3% of the time-period, i.e., the first 2 hours of the day.

Note that the quartile-based temporal distributions in Fig. 3 are generated under the assumption of the homogeneity of monthly precipitation. In the absence of monthly precipitation homogeneity, seasonality must be considered [59]. Hence, we follow the procedure described in Huff (42) to generate seasonal-based temporal distributions. As the input, we use 20 years of precipitation data (i.e., year 1997–year 2016) in the City of Knoxville, obtained from National Center for Environmental Information (NCEI) [15], stratified across the four seasons. Fig. 4 presents the resulting seasonal temporal distributions of daily precipitation.

Lastly, to analyze the homogeneity of monthly precipitation to determine whether quartile-based or seasonal-based temporal dis-

tributions can be applied to convert the daily projections into hourly projections, we use a variation of precipitation coefficient of variability [27,59]. Let p_k denote the accumulated precipitation in month k and let η denote the precipitation coefficient of variability. The value of η is given by

$$\eta = \frac{\sum_{k=1}^{12} p_k^2}{(\sum_{k=1}^{12} p_k)^2}.$$

If the value of η ranges between 0 and 0.1, it suggests that precipitation is relatively uniformly distributed across the months, i.e., homogeneity of monthly precipitation. In contrast, if the value of η ranges between 0.1 and 0.2, it indicates seasonal patterns for precipitation. Note that if the value of η is greater than 0.2, it indicates that there are distinct monthly precipitations and thus, monthly

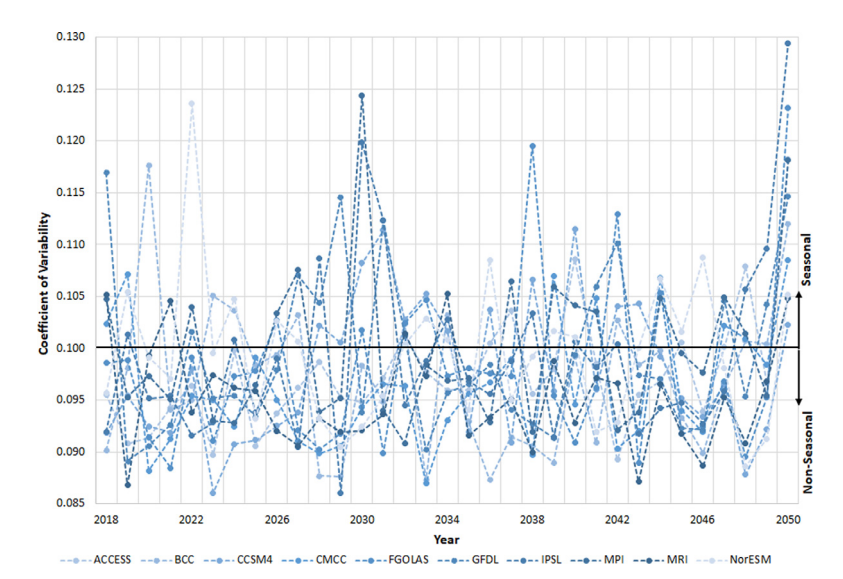


Fig. 5. Coefficient of variability for the ten precipitation projections for the City of Knoxville, for years 2018 to 2050.

precipitations are fully heterogeneous. Fig. 5 presents the coefficient of variability, η , for the 10 precipitation projections during the planning time horizon. As seen in the figure, η ranges from 0.085 to 0.125, and is always less than 0.2.

Finally, we use the following procedure to pre-process any given daily precipitation projection (from any of the ten CGCMs) to generate an hourly projection. First, we break down the daily precipitation projection by year. For any given year, we first examine the value of coefficient of variability to determine whether quartile-based or seasonal-based temporal distributions apply. If quartile-based distributions apply, we first determine the proportion of time that the highest percentage of precipitation occurred in the first-fourth quarters of the day using the historical precipitation data collected in the Ohio River Basin, which includes the City of Knoxville [20]. Next, for any given day of the year in the daily precipitation projections, we generate a weighted random number according to these proportions to determine which quartile to use. Next, we generate a weighted random number according to the probability of observing each of the cumulative distributions in the corresponding quantile. Finally, once a cumulative distribution is chosen, we use it to project the amount of precipitation in that day into an hourly time series. Similarly, if seasonal-based temporal distributions apply, for any given day in any given season, we generate a weighted random number according to the probability of observing each of the cumulative distributions for that season. We then use the selected cumulative distribution to project the amount of precipitation in that day into an hourly time series.

3.3. Hydrological simulations and estimating surface runoff

As discussed in Section 3.2, precipitation projections need to be fed into hydrological simulators to calculate the surface runoff during any given precipitation event, at various degrees of GI installation. In this study, to perform hydrological simulations we use EPA SWMM [63], a widely used software in literature [21,28,43,53,56,62,70,71]. Note that conducting brute-force SWMM simulations can be time-consuming. Hence, in this section, we first discuss the computational difficulties of executing such simulations and then provide an approach for sampling events to estimate the total baseline surface runoff, $Q_i^{\psi,t}$, and the surface runoff captured by GI practices, $\hat{Q}_{i,j,l}^{\psi,t}$, under various projected precipitation scenarios, ψ , for the stochastic model. Next, we describe the approach used for calculating the $100(1-\alpha)\%$

CIs for the amount of surface runoff captured by GI practices that gives the estimated value of $\hat{q}_{i,j,l}^{\psi,t}(\alpha)$ for the conservative-stochastic model. Finally, we describe the approach used for calculating the runoff adjustment factor $\beta_{i,j,l}^{i',j',l'}$ over any given downstream subcatchment.

SWMM partitions rainfall to runoff and routes it through the watershed and the potential GI practices, while accounting for several adjustments such as (i) rainfall interception from depression storage, (ii) infiltration of rainfall into unsaturated soil layers, and (iii) percolation of infiltrated water into groundwater layers [63]. Note that SWMM simulation can be extremely computationally expensive, given a large watershed and a long time horizon for the input precipitation. For instance, based on our experiments, each SWMM simulation performed on a 2.4 GHz CPU (single core) to obtain the surface runoff after placing GI practices within a single sub-catchment can take on the order of approximately 25 minute to execute for a time series that spans only one year, expressed in hourly units. Note that increasing the planning horizon proportionally increases the simulation time. In addition, given the total number of the sub-catchments, |V|, the number of GI types to place in each sub-catchment, |G|, and the number of possible installation levels, |L|, a total of $(|G| \cdot |L| + 1)^{|V|}$ SWMM simulations must be executed to calculate the surface runoff for all possible combinations of GI placements if all sub-catchments are hydrologically connected. Hence, using a brute-force simulation approach is computationally intractable even for a medium-sized watershed, with approximately 100 sub-catchments.

Therefore, in this study, we exploit three approaches to mitigate the prohibitively long simulation time to estimate the surface runoff. First, we use a sampling method to approximate surface runoff resulting from precipitation scenarios using only a series of sampled events instead of the entire precipitation time series spanning the planning horizon. Note that we use the sampling method along with bootstrapping to also calculate CIs for the estimated surface runoff volumes. Second, we run SWMM simulations for all sub-catchments simultaneously, i.e., we execute one simulation under no GI practice placement to calculate the baseline surface runoff over all sub-catchments, and a total of $|G| \cdot |L|$ simulations where the same GI practice of type j in the same level l is placed within all sub-catchments to calculate the corresponding runoff after placement. Clearly, if hydrological connectivity among sub-catchments are not captured in the watershed model, the estimated runoff volumes give the parameters $Q_i^{\psi,t}$ and $\hat{Q}_{i,l,j}^{\psi,t}$, respectively. However, if hydrological connectivity among sub-catchments are captured in the watershed model, the former and latter groups of estimated runoff volumes need to be adjusted back by the adjustment factor $\beta_{i,j,l}^{i',j',l'}$ to estimate the parameters $Q_i^{\psi,t}$ and $\hat{Q}_{i,l,j}^{\psi,t}$, respectively. In our main SWMM simulation model for the watershed, the hydrological connectivity among sub-catchments is not entirely captured, which simplifies the estimation of $Q_i^{\psi,t}$ and $\hat{Q}_{i,l,j}^{\psi,t}$. However, at the same time, it complicates the process of estimating the adjustment factors $\beta_{i,j,l}^{i',j',l'}$. To be able to estimate the adjustment factors, we develop a complementary SWMM model, which we calibrate based on the characteristics of the sub-catchments and their hydrological connectivity in the watershed. Lastly, we stratify sub-catchments based on their characteristics and only calculate the adjustment factors $\beta_{i,j,l}^{i',j',l'}$ for a reduced number of sub-catchment type pairs using the set of sampled events.

Sampling events and calculating surface runoff parameters, $Q_i^{\psi,t}$ and $\hat{Q}_{i,l,j}^{\psi,t}$, for the stochastic model. As discussed in Section 2, precipitation intensity, i.e., the amount of precipitation in a period of time, is an important predictor of, and is negatively correlated with, GI practice performance. Depending on the intensity of precipitation events, a GI practice may present different performance levels. For instance, GI practices generally exhibit a lower performance under a series of short but intense events, but a higher performance under long but mild events. Hence, we use precipitation intensity as a basis for sampling events.

Recall that $\hat{\psi} \in \hat{\Psi}$ denotes daily precipitation projection time series produced by the CGCMs, and $\psi \in \Psi$ denotes hourly precipitation projection time series, corresponding to scenarios in the stochastic model. As discussed in Section 3.2, the hourly precipitation projection time series, ψ , resulting from a daily precipitation projection time series, $\hat{\psi}$, is not unique. In fact, each of the resulting hourly precipitation projection time series can have very different daily precipitation intensities in any given day. Therefore, we rely on repeated sampling to produce a large set of hourly precipitation projection time series, ψ , and then aggregate them based on precipitation intensities to estimate runoff volumes. The detailed steps are as follows.

- **Initialization**: For each of the ten daily precipitation projections, $\hat{\psi} \in \hat{\Psi}$, use precipitation coefficient of variability, η , to identify the relevant set of temporal distributions for any given rainy day, i.e., when precipitation volume is greater than zero, over the span of 32 years, i.e., 2018–2050. Next, for each of these rainy days, randomly select from the corresponding set of temporal distributions to project daily precipitation into hourly basis. Repeat the procedure to generate 100 time series of hourly precipitation projections for each of the 10 daily precipitation projections, $\hat{\psi} \in \hat{\Psi}$. This results in 1000 time series of hourly precipitation projections, $\psi \in \hat{\Psi}$, each of which consist of a series of hourly precipitation events with various intensities.
- **Aggregation**: Use all $\psi \in \Psi$ to calculate the histogram of hourly event intensities, using Sturges rule to break the intensity range into categories.
- **SWMM Simulation**: For any given 100 hourly precipitation projections corresponding to daily precipitation projection $\hat{\psi}$, calculate the histogram of hourly event intensities using the previously defined categories. Randomly select a set of 10 events from the category to use in SWMM simulations. If a category has fewer than 10 events, use all in the simulation. For any chosen event, execute SWMM simulation when no GI practice is placed in any of the watershed subcatchments, $i \in V$. For any given sub-catchment, calculate

- the category's corresponding baseline average 'volume-based runoff coefficient,' i.e., the ratio of runoff volume to the precipitation volume [39], using all selected events in the category. Next, for any selected event, execute SWMM simulation when identical GI practice j in level l is placed across all sub-catchments. For any given sub-catchment i, calculate the category's corresponding average 'runoff coefficient' with respect to the placed GI practice of type j with level l, using all selected events in the category. Follow the procedure for all $\hat{\psi} \in \hat{\Psi}$ and calculate all runoff coefficients.
- Estimating Runoff: Given an hourly precipitation projection $\psi \in \Psi$ for sub-catchment $i \in V$, use the expanded rational method [39] to calculate the baseline runoff using the corresponding baseline runoff coefficients of the corresponding daily precipitation projection $\hat{\psi} \in \hat{\Psi}$. That is, for any given rainy day in the projection $\psi \in \Psi$, calculate the total daily runoff by multiplying the runoff volume by the runoff coefficient that corresponds to the precipitation intensity in that day, obtained from the corresponding $\hat{\psi} \in \hat{\Psi}$. The overall yearly baseline runoff for the hourly precipitation projection ψ over sub-catchment i, i.e., $Q_i^{\psi,t}$ for all $0 \le t \le T$, is the summation of calculated total daily runoff volumes in that year. Use the same method to calculate the overall runoff for sub-catchment $i \in V$ with respect to placed GI practice $j \in G$ in level $l \in L$ in year $t \leq T$. Let $\tilde{Q}_{i,l,j}^{\psi,t}$ denote the surface runoff over sub-catchment $i \in V$ given that GI practice of type $j \in G$ is installed in level $l \in L$ within the sub-catchment under the hourly precipitation projection $\psi \in \Psi$ in year t. Hence, under hourly precipitation projection ψ , the corresponding surface runoff captured by the GI practice, $\hat{Q}_{i,j,l}^{\psi,t}$, for all $i \in V$, $j \in G$, $l \in L$, $0 \le t \le T$ is obtained as follows: $\hat{Q}_{i,j,l}^{\psi,t} = Q_i^{\psi,t} - \tilde{Q}_{i,l,j}^{\psi,t}$. Repeat this process for all 1000 hourly precipitation projections to estimate the corresponding surface runoff volumes $Q_i^{\psi,t}$ and $\hat{Q}_{i,j,l}^{\psi,t}$ for all sub-catchments in

Fig. 6 presents the variation in the estimated volume-based runoff coefficient across all sub-catchments in our watershed of interest under various GI practice installation. BR and RG stand for bioretention and rain garden, respectively, and the three levels of installation are described in Section 3.1. As seen in the figure, the runoff coefficient is generally lower after installing GI practices, compared with the baseline (i.e., no treatment). In addition, bioretention generally have a lower runoff coefficient, hence present a better performance in reducing runoff compared with rain gardens. Lastly, the larger the GI practice, especially in bioretentions, the higher the performance.

Calculating confidence intervals for runoff volumes for the conservative-stochastic model. Recall that the conservative-stochastic model requires the $100(1-\alpha)\%$ CIs for surface runoff for any given GI practice in any given sub-catchment. We use bootstrapping to generate these intervals [31]. In contrast to stochastic model in which we use a total of 1000 hourly precipitation projections as scenarios to estimate the corresponding surface runoff volumes, in the conservative-stochastic model we redefine scenarios to be the aggregate measure of 100 hourly precipitation projections produced from any given CGCM. We then use these scenarios to estimate the runoff volumes as follows.

First, we follow the first three steps in the procedure used for calibrating the stochastic model, i.e., Initialization, Aggregation, and SWMM Simulation, from which we obtain volume-based runoff coefficients for all identified categories for any given CGCM. Next, for each CGCM, we group all volume-based runoff coefficients regardless of the categories and use bootstrapping to replicate large enough bootstrap samples to calculate the corresponding

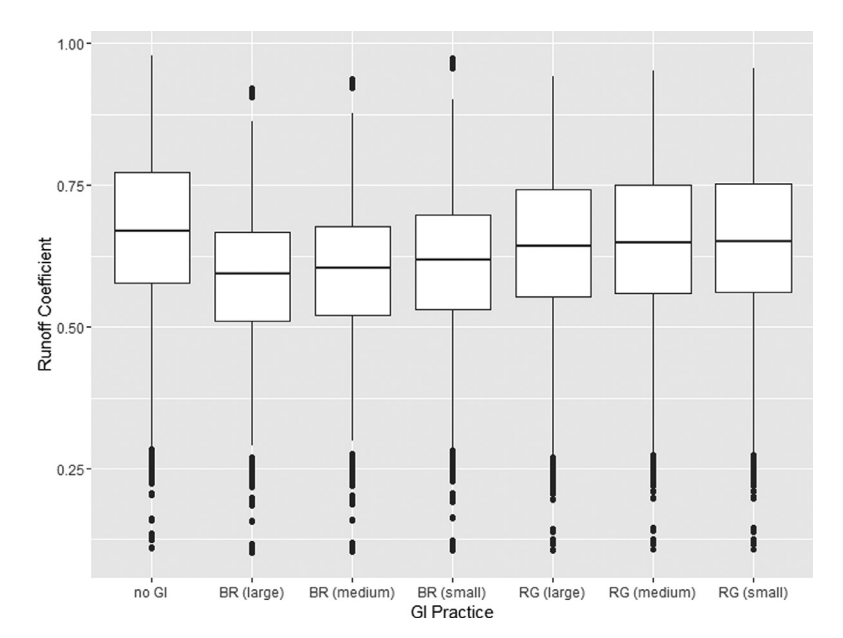


Fig. 6. Boxplots of the estimated volume-based runoff coefficients for all sub-catchments in the watershed of interest, for all given hourly precipitation projections corresponding to CGCM ACCESS over the years 2018–2050, under various GI practice installation. BR and RG stand for bioretention and rain garden, respectively. The three levels of installation are described in Section 3.1.

 $100(1-\alpha)\%$ CI for runoff coefficients for each sub-catchment, under all GI practice placement (and no treatment). Finally, we use the center and half of the width of each CI in the rational method to estimate the corresponding $\hat{Q}_{i,l,j}^{\psi,t}$ and $\hat{q}_{i,l,j}^{\psi,t}(\alpha)$.

Calculating runoff adjustment factor, $\beta_{i,j,l}^{i',j',l'}$. As discussed in

Section 2, the surface runoff volume over a downstream subcatchment is not only a function of the amount of precipitation, the sub-catchment's hydorlogical characteristics, and the placed GI practices within the sub-catchment, but also it is affected by (large-scale) GI practices placed within upstream subcatchment(s) that are hydrologically connected to this downstream sub-catchment. Also recall that we assume the adjustments over downstream sub-catchments are additive when large-sale GI practices are placed within more than one of its upstream subcatchments. As discussed earlier in this section, our main SWMM simulation model for the watershed does not capture the entire hydrological connectivity among sub-catchments. Hence, to be able to estimate the adjustment factors, we develop a complementary SWMM model, which we calibrate based on the characteristics of the sub-catchments and their hydrological connectivity in the watershed.

Specifically, we develop a SWMM model that consists of two hydrologically connected sub-catchments, where the residual runoff from the upstream sub-catchment flows onto the downstream sub-catchment. We run the simulation for any given pairs of sub-catchment characteristics to estimate the adjustment factor, $\beta_{i,j,l}^{i',j',l'}$, under various GI practice placements as well as no treatment. To further reduce the computation time, we only use the most important sub-catchment characteristics related to runoff reduction, as identified in the literature [24], and stratify sub-catchments accordingly (see Appendix E for details).

Fig. 7 presents a subset of the estimated runoff adjustment factors over the downstream sub-catchment, where a large bioretention is placed in upstream and a small bioretention is placed downstream, for all observed combinations of sub-catchment characteristics as described in Appendix E. Sub-catchment characteristics are shown as tuples, where the three elements correspond to percent of imperviousness, percent of slope, and Manning's n for overland flow over the pervious portion of the sub-catchment, each

of which are categorized into three levels of 0–2, encoding low, medium, and high, respectively. As seen in the figure, the adjustment factor varies based on the characteristics of the pair of subcatchments, ranging between 0.2% and 0.75%. In general, a higher level of imperviousness results in a larger amount of runoff. Hence, when the upstream sub-catchment has a higher level of imperviousness, it contributes a larger amount of flow onto hydrologically connected downstream sub-catchments. As a result, and as seen in the figure, placing a large bioretention in a highly impervious upstream sub-catchment contributes to a larger adjustment in runoff over the downstream sub-catchment. In contrast, the impact is less pronounced when the upstream sub-catchment is relatively pervious.

4. Case study

In this section, we first conduct a case study for a watershed in a mid-sized city in the U.S. We then conduct sensitivity analysis, investigate the relationship between 1-neighbor constraint and the runoff adjustment factor, discuss the findings and provide insights on the implications of our modeling approaches.

For computational experiments we use the IBM ILOG CPLEX 12.8 (64-bit edition) on a PC running Microsoft Windows 7 (64-bit edition) with a Core i7, 4 GHz processor and 32 Gigabyte of RAM. In general, solving a stochastic model is much harder than solving a conservative-stochastic model. On average, the computational time of two-stage stochastic models is on the order of 3–4 minutes, which is approximately two orders of magnitude larger than that of two-stage conservative-stochastic models, which takes on the order of 1 second to solve. Moreover, solving a multi-stage conservative-stochastic model is much harder than solving a two-stage conservative-stochastic model. On average, the computational time of multi-stage conservative-stochastic model is 14 folds larger than that of two-stage conservative-stochastic model.

4.1. Case study specifications

As a case study, we consider the First Creek in the City of Knoxville, Tennessee. The creek is located entirely within the City of Knoxville and have been identified as the principal sources

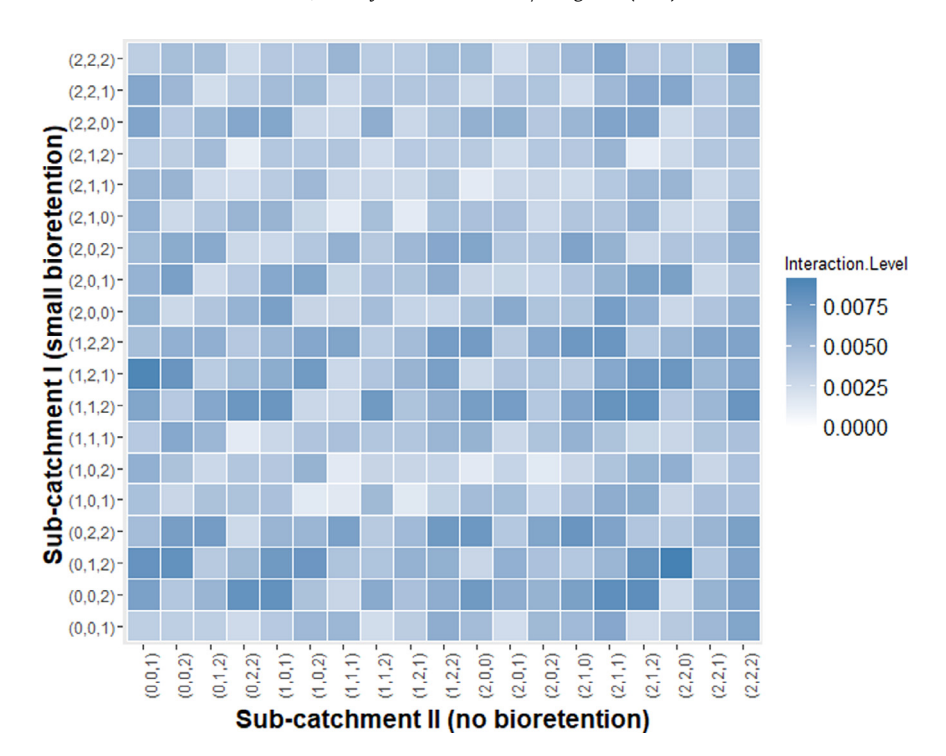


Fig. 7. Heat map of the runoff adjustment factors over the downstream sub-catchment, where a large bioretention is placed in upstream and a small bioretention is placed downstream, for all observed combinations of sub-catchment characteristics' categories as described in Appendix E. Sub-catchment characteristics are shown as tuples, where the three elements correspond to percent of imperviousness, percent of slope, and Manning's n for overland flow over the pervious portion of the sub-catchment, each of which are categorized into three levels of 0–2, encoding low, medium, and high, respectively.

of flooding in Knox County, Tennessee [36]. The watershed's combined area is 14805 acres and encompasses parts of the most densely populated regions of the city, including Downtown Knoxville. The First Creek hydrological model was provided to us by the Stormwater Engineering Division of the City [58]. The hydrological model divides the creek into 140 sub-catchments, all of which are associated with one rain gauge. This model also includes 365 junction nodes and 439 conduit links that direct the flow into the Tennessee River.

Fig. 8 illustrates the map of land cover (left panel) and hydrological sub-catchments (right panel) of the First Creek. The red shades on the left panel represent level of development, from low (mostly meadow and forest land cover) to high. As seen in the figure, the southern region of the watershed, which is where Downtown Knoxville is located, is highly developed. Subsequently, this dense region has larger amount of impervious area, compared with other regions in the watershed (see Appendix F for more details).

In this case study, we use a planning horizon of length 33 years (T=33), i.e., for years 2018–2050, for which the precipitation projections are available. First, in Section 4.2, we compare the two-stage stochastic and conservative-stochastic models with restricted decision sets. We let the first and second stage decision variables be respectively taken in the beginning of the planning horizon, i.e., in year 2018, and 10 years into the planning horizon, i.e., in year 2027 ($\overline{T}=10$), and conduct sensitivity analysis to draw insights. Next, in Section 4.3 we use the two-stage stochastic and the two-stage conservative-stochastic models from Section 4.2 to investigate the relationship between 1-neighbor constraint and the runoff adjustment factor.

Next, in Section 4.4 we use the two-stage conservativestochastic model from Section 4.2 and add chance constraints, as described in Section 2.3, to evaluate the impact of incorporating sub-catchment-level runoff reduction considerations on the results.

Finally, in Section 4.5, we compare the results of the two-stage and three-stage conservative-stochastic models with relaxed decision sets. In the three-stage model, the 33-year planning horizon is divided into three 11-year periods, and GI placement occurs at the beginning of each period.

4.2. Two-stage models: Stochastic vs conservative-stochastic

In this section, we compare the two-stage stochastic and conservative-stochastic models with restricted decision sets. That is, large-scale and small-scale practices can only be placed in the first and second stages, respectively, before and after a scenario is realized.

Given the 1000 generated hourly precipitation time projections discussed in Section 3.3, we let Φ_S denote the projected total expected runoff volume, i.e., $\Phi_S = \sum_{\psi \in \Psi} \pi^{\psi} \cdot \sum_{i \in V} \sum_{0 \le t \le T} Q_i^{\psi, t}$, over the First Creek equals 4.57×10^{11} gallons. This volume is used as total baseline surface runoff under no treatment (i.e., no GI practice placed) in the stochastic model. For the conservative-stochastic model, given the same projections that are aggregated regardless of their daily precipitation intensity categories, we let $\Phi_{R_{\alpha}}$ denote the sample average baseline surface runoff under $100(1-\alpha)\%$ confidence level. Accordingly, for the given scenarios, $\Phi_{R_{0.05}}=4.56\times$ 10¹¹ and the estimated 95% CI for the expected baseline surface runoff equals $4.56 \times 10^{11} \pm 1.75 \times 10^{9}$. Note that these runoff volumes correspond to no treatment (i.e., no GI practice placed) in the conservative-stochastic model. In our computational results, we report the percentage reduction in total expected runoff volume under the optimal GI practice placement across the watershed, i.e., $\left(\Phi_S - \phi_S(\chi_S^\star)\right)/\Phi_S$ and $\left(\Phi_{R_{0.05}} - \phi_{R_{0.05}}(\chi_R^\star)\right)/\Phi_{R_{0.05}}$ for the stochastic and conservative-stochastic models, respectively.

First, we solve the models under the available budgets of 10, 20, and 50 million dollars and compare the corresponding optimal GI practice placements. Fig. 9 presents the first stage decision variables under the optimal solution for all cases considered. That is, it presents the sub-catchments in which bioretentions are placed and their level of installation. In addition, Table 1 summarizes the

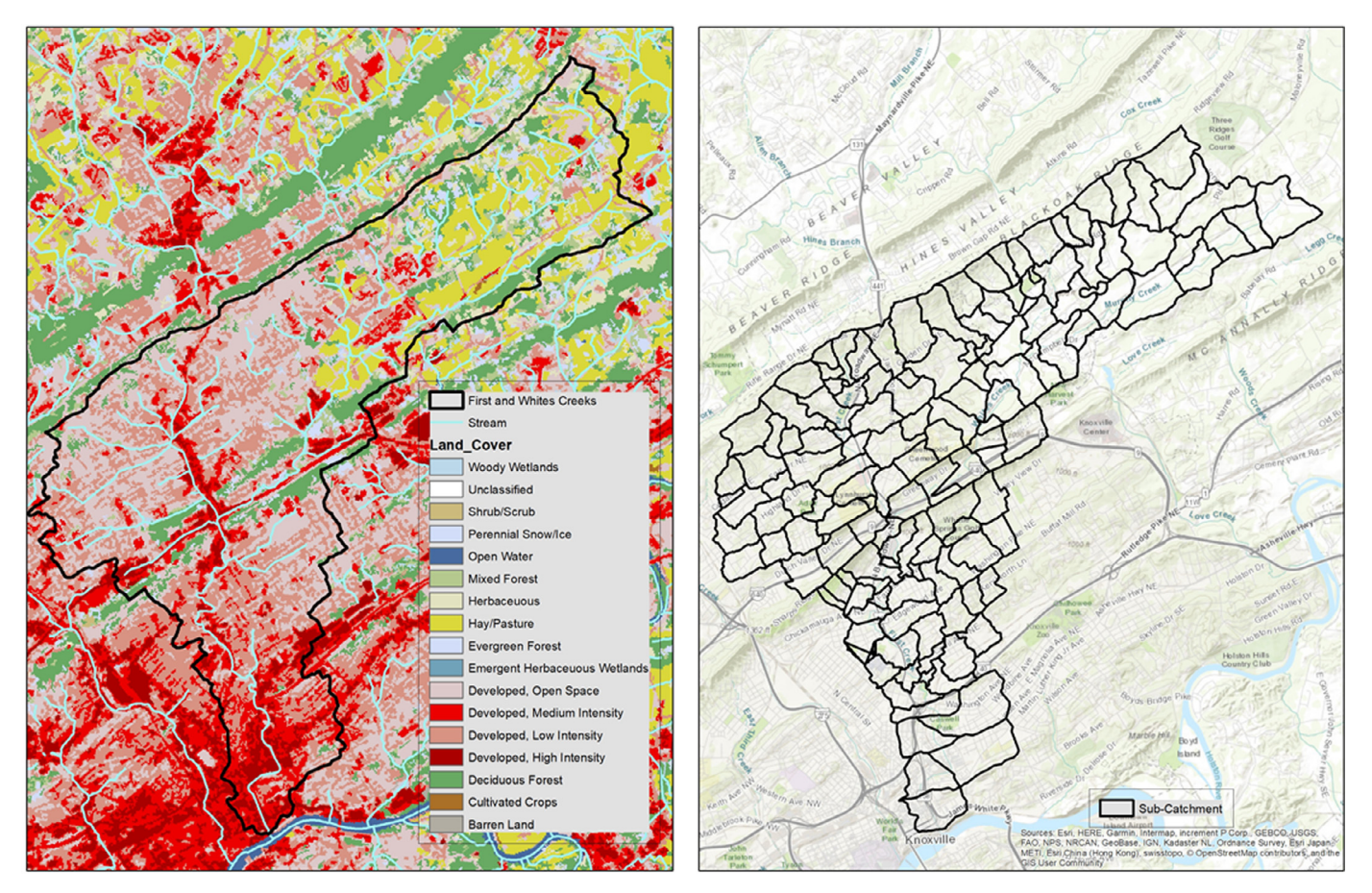


Fig. 8. Map of land cover [41] (left panel) and hydrological sub-catchments (right panel) of the First Creek, Knoxville, Tennessee.

Table 1Average percentages of sub-catchments in which rain gardens are placed, along with the distribution of their level of installation, given that the scenarios from one of the ten CGCMs are realized (second stage decision variables) for various levels of available budget.

		Budget											
Model		10 million dollars				20 million dollars				50 million dollars			
	CGCM	% of Sub-Cat.	Large	Med.	Small	% of Sub-Cat.	Large	Med.	Small	% of Sub-Cat.	Large	Med.	Small
Stochastic	ACCESS	64.1%	11.1%	3.8%	85.1%	47.6%	54.4%	4.2%	41.4%	23.6%	67.3%	10.8%	21.9%
	BCC	63.7%	11.0%	4.8%	84.3%	49.7%	45.3%	13.4%	41.3%	23.4%	70.4%	6.9%	22.7%
	CCSM4	67.1%	9.6%	1.0%	89.4%	53.1%	40.0%	10.9%	49.1%	23.4%	69.6%	7.6%	22.8%
	CMCC	66.4%	5.5%	10.5%	84.0%	52.9%	39.1%	13.7%	47.2%	23.6%	72.7%	0.0%	27.3%
	FGOALS	67.0%	9.6%	1.3%	89.1%	51.0%	46.1%	6.4%	47.4%	23.6%	69.7%	6.1%	24.2%
	GFDL	57.2%	16.1%	8.9%	75.0%	52.8%	39.3%	13.4%	47.3%	23.6%	70.2%	5.1%	24.7%
	IPSL	65.4%	8.2%	7.0%	84.8%	49.2%	49.0%	8.1%	42.9%	22.9%	74.4%	4.3%	21.4%
	MPI	66.3%	5.2%	11.3%	83.5%	47.0%	53.5%	8.9%	37.6%	22.9%	74.9%	3.3%	21.8%
	MRI	54.4%	20.6%	7.3%	72.2%	45.7%	56.3%	9.4%	34.4%	22.6%	68.6%	19.3%	12.1%
	NorESM	68.2%	7.3%	3.6%	89.1%	52.3%	42.3%	9.3%	48.4%	23.1%	71.2%	8.3%	20.6%
Conservative-	ACCESS	80.0%	43.8%	9.8%	46.4%	72.9%	51.0%	7.8%	41.2%	40.0%	60.7%	8.9%	30.4%
stochastic	BCC	82.1%	43.5%	5.2%	51.3%	74.3%	51.0%	3.8%	45.2%	40.7%	61.4%	3.5%	35.1%
	CCSM4	81.4%	42.1%	9.6%	48.2%	73.6%	49.5%	8.7%	41.7%	38.6%	66.7%	5.6%	27.8%
	CMCC	84.3%	39.8%	7.6%	52.5%	75.7%	47.2%	7.5%	45.3%	40.7%	59.6%	7.0%	33.3%
	FGOALS	84.3%	41.5%	4.2%	54.2%	77.1%	46.3%	5.6%	48.1%	40.7%	63.2%	0.0%	36.8%
	GFDL	82.9%	41.4%	7.8%	50.9%	74.3%	49.0%	7.7%	43.3%	39.3%	63.6%	7.3%	29.1%
	IPSL	83.6%	41.0%	6.8%	52.1%	75.7%	48.1%	5.7%	46.2%	40.7%	61.4%	3.5%	35.1%
	MPI	82.9%	38.8%	12.9%	48.3%	74.3%	47.1%	11.5%	41.3%	39.3%	63.6%	7.3%	29.1%
	MRI	83.6%	40.2%	8.5%	51.3%	75.0%	47.6%	8.6%	43.8%	40.0%	62.5%	5.4%	32.1%
	NorESM	82.9%	40.5%	9.5%	50.0%	74.3%	47.1%	11.5%	41.3%	40.0%	60.7%	8.9%	30.4%

second stage decision variables under the optimal solution for all cases considered. That is, it presents the average percentages of sub-catchments in which rain gardens are placed, along with the distribution of their level of installation, given that the scenarios from one of the ten CGCMs are realized. As expected, and seen in the figure and table, as the available budget increases, a larger

number of sub-catchments are selected for bioretention installation in the first stage and the sizes of placed rain gardens stochastically increases in the second stage, under all scenarios generated from the ten CGCMs.

Recall that the unit construction cost of bioretentions (and rain gardens) are equal across all sub-catchments. However, as dis-

15

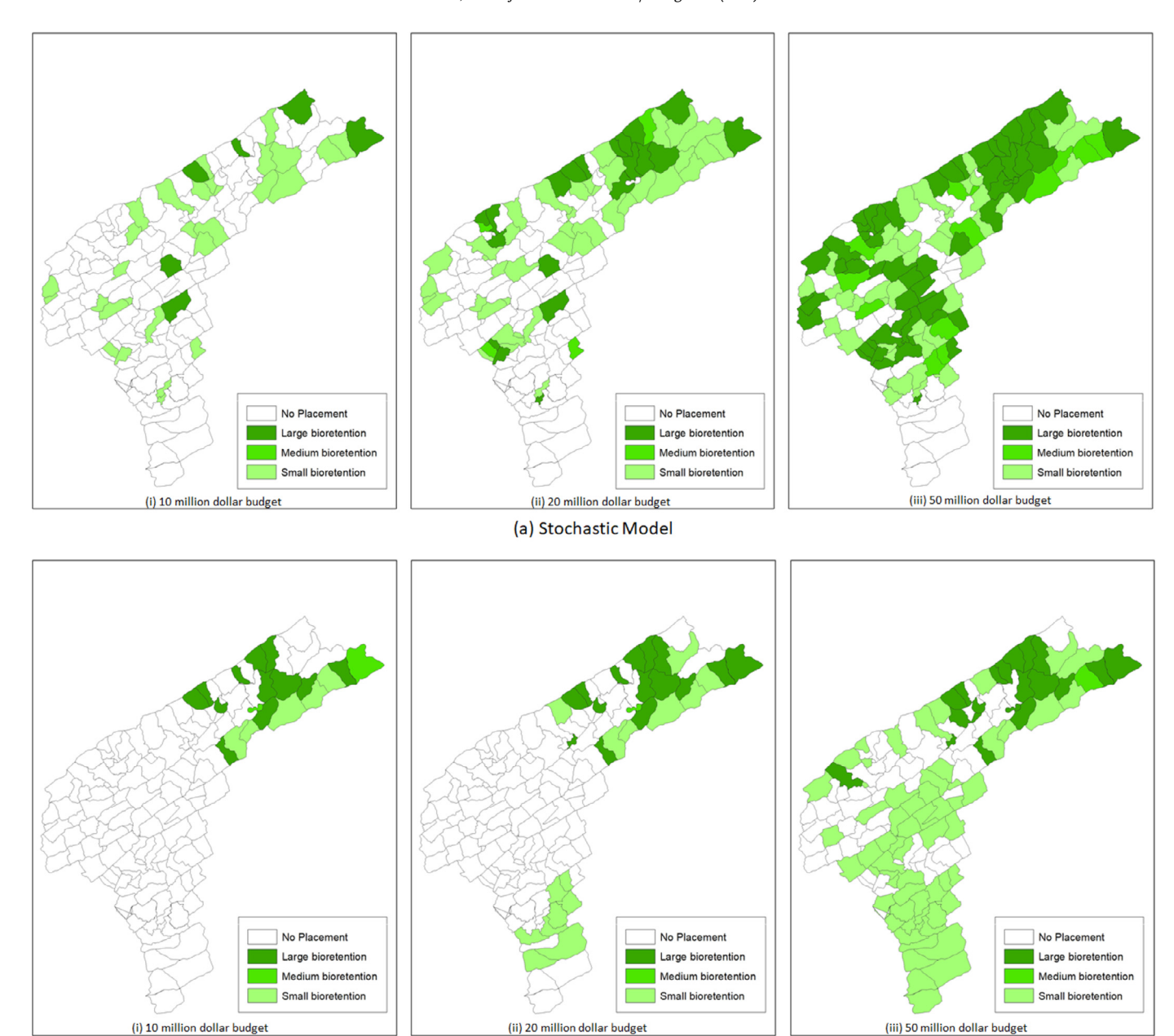


Fig. 9. Map of placed bioretentions and their level of installation (first stage decision variables) under the optimal solution for various levels of available budget.

(b) Conservative-stochastic Model

cussed in Section 3.1, the area used for bioretention installation corresponds to the level of imperviousness in that sub-catchment, i.e., a fixed percentage of the impervious area of the sub-catchment is treated with bioretentions. As a result, it is much more expensive to place bioretentions in highly developed sub-catchments as the level of development largely correlates with the level of imperviousness. Therefore, in Fig. 9, sub-catchments in the southern region of the watershed, where the highly developed Downtown Knoxville is located, are not usually selected for bioretention installation. Indeed, as seen in the figure, given a limited budget, e.g., 10 million dollars, solutions to both stochastic and conservative-stochastic models consist of placing bioretention in sub-catchments with a low level of development, where the construction cost is generally lower. Recall that in both models, the 1-neighbor constraint on first stage decision variables ensures connectivity among large-scale GI practice placements. Therefore, if a highly developed sub-catchment is selected as part of the first

stage decisions, the available budget should be enough to cover the costs of placing bioretentions not only in that sub-catchment, but also in at least one of its hydrologically connected neighbors. This, in turn, makes placing bioretentions in general very costly within highly developed regions, e.g., sub-catchments in the southern region of the watershed, where the highly developed Downtown Knoxville is located. Accordingly, only as the amount of available budget increases, it becomes optimal to place bioretentions in some of the more developed sub-catchments. It is interesting to note that some of the placed bioretentions in Fig. 9 are stand-alone. Note that this does not violate the 1-neighbor constraint as these sub-catchments are not downstream to any of their neighboring sub-catchments, i.e, they have no upstream hydrologically connected sub-catchments and hence, 1-neighbor connectivity constraint does not apply to them.

As seen in Fig. 9, the solutions to the stochastic and conservative-stochastic models are not necessarily identical under

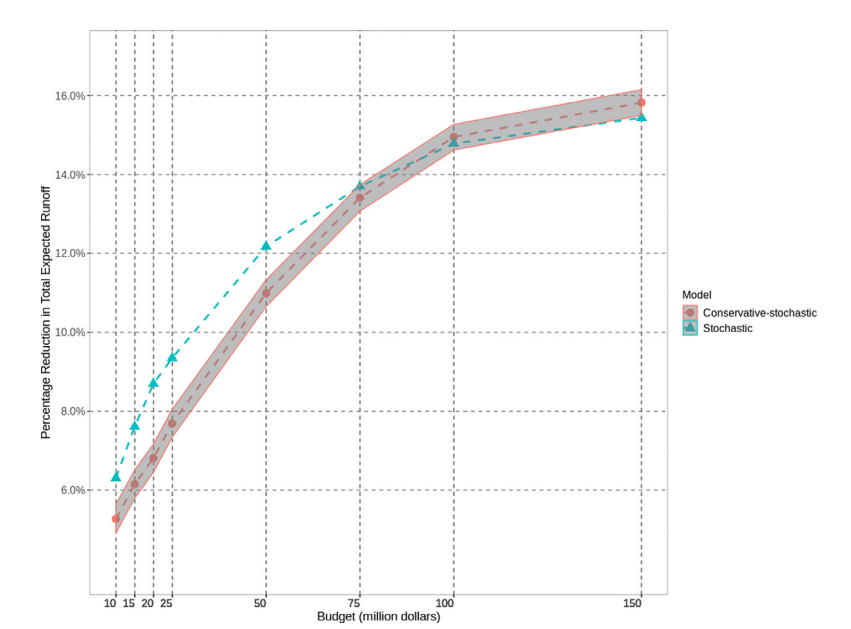


Fig. 10. Comparison of percentage reduction in total expected runoff under two-stage stochastic and conservative-stochastic models, where the available budget ranges between 10 and 150 million dollars. The shaded area represents the 95% CI for reduction in total expected runoff for the conservative-stochastic model.

the given available budget; however, comparing the results shows similar reduction in total expected surface runoff over the planning horizon for the two models. For instance, under 50 million dollars available budget, the optimal GI placement contributes to 12.01% and 11.30% reduction in total expected runoff for the stochastic and conservative-stochastic models, respectively. It is interesting to note that these reductions are achieved under different allocations of budget in the first and second stages under the two models. Specifically, in the stochastic model, the percentages of budget spent in the first stage are 81%, 88%, and 97% under 10, 20, and 50 million dollars available budget, respectively. Compare these percentages, respectively, with 64%, 82%, and 96% spent in the first stage in the conservative-stochastic model. This suggests a slightly more conservative allocation of budget in the first stage under the conservative-stochastic model, compared with the stochastic model, especially when the available budget is relatively low. As seen in Table 1, this relatively conservative allocation of budget is compensated for in the second stage, where the average percentages of sub-catchments in which GI practices are placed is generally larger under the conservative-stochastic model, compared with the stochastic model, across the scenarios generated from the ten CGCMs.

Next, we more extensively compare the percentage reduction in total expected runoff under the stochastic and conservativestochastic models. Fig. 10 presents a comparison of percentage reduction in total expected runoff under stochastic and conservativestochastic models, where the available budget ranges between 10 and 150 million dollars. The shaded area represents the 95% CI for reduction in total expected runoff for the conservative-stochastic model. Note that in reporting the percentage reduction in total expected runoff under the conservative-stochastic model, we use the center of the 95% CI, as depicted in the figure. As seen in Fig. 10, the stochastic model performs relatively better under lower budgets, i.e., 75 million dollars or less. For instance, under 20 million dollars available budget, the stochastic model outperforms the conservative-stochastic model by 1.89% reduction in total expected runoff. However, this difference between the objective values decreases in the amount of available budget and at higher budgets, the conservative-stochastic model performs relatively better than the stochastic model. For instance, under 150 million dollars available budget, the conservative-stochastic model outperforms the stochastic model by 0.39% reduction in total expected runoff.

We conducted analyses to examine the sensitivity of the solutions with respect to some of the important calibrated parameters, including the years to realize a scenario, \overline{T} , the ratio of maintenance cost to construction cost, ρ , and the runoff adjustment factor, $\beta_{i,i,l}^{i',j',l'}$ on two-stage stochastic models. In both models, realizing a scenario sooner, i.e., smaller values of \overline{T} , results in a larger reduction in total expected runoff. However, overall, the differences among the percentage runoff reductions with respect to various values for \overline{T} , ranging from 5 to 15, is low and decreases in the amount of available budget. Similarly, as expected, given any available budget, the percentage runoff reduction non-increases in ρ , where as the budget increases, the impact of ρ on the percentage runoff reduction diminishes. Finally, in contrast, connectivity, captured through adjustment factors, $\beta_{i,j,l}^{i',j',l'}$, contributes to reduction in total runoff under various available budgets, where connectivity contributes to a higher percentage of runoff reduction under higher levels of available budget. The detailed sensitivity analyses results are available in Appendix G.

4.3. Investigating the relationship between 1-Neighbor constraint and the runoff adjustment factor

In this section, we evaluate the importance of accounting for the adjustment in surface runoff reduction due to GI placements in connected sub-catchments using the runoff adjustment factor, $\beta_{i,j,l}^{l',j',l'}$. In this section, for simplicity of notation, we let $\beta = [\beta_{i,j,l}^{l',j',l'}]$ denote the vector of all adjustment factors. Specifically, we evaluate the expected opportunity loss due to installing a potentially sub-optimal solution as a result of not accounting for runoff adjustment factors. We conduct the analyses with and without considering the 1-neighbor constraint to draw insights.

First, let $\tilde{\chi}_S \in \Omega$ denote the optimal solution of the stochastic model, where all adjustment factors are set to zero in the stochastic objective function (1), i.e., $\tilde{\chi}_S = arg\min_{\chi \in \Omega} \phi_S(\chi; \beta = 0)$. Similarly, let $\tilde{\chi}_R \in \Omega$ denote the optimal solution of the conservative-stochastic model, where all adjustment factors are set to zero in the conservative-stochastic objective function (10), i.e., $\tilde{\chi}_R = 0$

Table 2 Percentage reduction in total expected runoff volume under the solutions χ_M^{\star} , χ_M' , and $\overline{\chi}_M$, $M \in \{S, R\}$, where the budget available ranges between 10 and 150 million dollars. The corresponding values under $\tilde{\chi}_M$ and χ_M^{\star} , $M \in \{S, R\}$, are the same; hence the former are not included in the table.

Budget (million dollars)	Stochastic			Conservative-stochastic			
	$\frac{\Phi_S - \phi_S(\chi_S^{\star})}{\Phi_S}$	$\frac{\Phi_S - \phi_S(\chi_S')}{\Phi_S}$	$\frac{\Phi_S - \phi_S(\overline{\chi}_S)}{\Phi_S}$	$\frac{\Phi_{R_{0.05}} - \phi_{R_{0.05}} \left(\chi_{R}^{\star}\right)}{\Phi_{R_{0.05}}}$	$\frac{\Phi_{R_{0.05}} - \phi_{R_{0.05}}(\chi_R')}{\Phi_{R_{0.05}}}$	$\frac{\Phi_{R_{0.05}} - \phi_{R_{0.05}}(\overline{\chi}_R)}{\Phi_{R_{0.05}}}$	
10	6.22%	7.71%	7.16%	5.30%	5.34%	5.34%	
15	7.55%	8.41%	8.40%	6.09%	6.16%	6.16%	
20	8.56%	9.25%	9.25%	6.87%	6.95%	6.95%	
25	9.33%	9.96%	9.95%	7.64%	7.72%	7.70%	
50	12.14%	12.41%	12.40%	10.97%	11.01%	10.99%	
75	13.71%	13.90%	13.90%	13.47%	13.47%	13.47%	
100	14.74%	14.84%	14.83%	14.86%	14.86%	14.86%	
150	15.37%	15.37%	15.37%	15.77%	15.77%	15.77%	

 $argmin_{\chi\in\Omega}\phi_R(\chi;\beta=0)$. Recall that χ_S^\star and χ_R^\star denote the optimal solutions of the stochastic and conservative-stochastic models under the estimated values for the adjustment factors, respectively. Clearly, $\phi_S(\chi_S^\star) \leq \phi_S(\tilde{\chi}_S)$ and $\phi_R(\chi_R^\star) \leq \phi_R(\tilde{\chi}_R)$, where the equalities respectively hold when $\tilde{\chi}_S$ and $\tilde{\chi}_R$ are optimal solutionsto the calibrated models with $\beta \geq 0$.

It is interesting to note that per our numerical experiments, both $\tilde{\chi}_S$ and $\tilde{\chi}_R$ are indeed optimal solutions to their corresponding models, i.e., $\phi_S(\tilde{\chi_S}) = \phi_S(\chi_S^\star)$ and $\phi_{R_{0.05}}(\tilde{\chi_R}) = \phi_{R_{0.05}}(\chi_R^\star)$, where χ_S^{\star} , $\tilde{\chi_R} \in \Omega$, specifically when the 1-neighbor constraint is included in the models. Our intuition is that because 1-neighbor connectivity constraint (7) enforces placing large-scale GI practices (firststage decisions) in hydrologically connected sub-catchments, it protects the solution to remain optimal, regardless of accounting for adjustment factors. Note that in our watershed of interest, there are only five sub-catchments (out of a total of 140 sub-catchments) that have more than one upstream sub-catchments; these five subcatchments each have exactly two upstream sub-catchments. Surprisingly, for all these five sub-catchments, the adjustment factors of the two upstream sub-catchments are rather identical. This further reduces the importance of including the exact adjustment factors in the model. Hence, we conclude that for our watershed of interest, given the structure of the corresponding graph $\mathbb{G}(V, A)$, enforcing the 1-neighbor constraint (7) is enough to obtain the optimal solution, contributing to a dramatic reduction in calibration efforts.

To further verify this hypothesis, we replicate the analysis without accounting for the 1-neighbor constraint (7). Specifically, we let χ_S' and $\overline{\chi}_S$ denote the optimal solutions to the stochastic model under the estimated values for the adjustment factors and where all adjustment factors are zero, respectively, when relaxing the 1-neighbor constraint (7), i.e.,

$$\chi_{S}' = \underset{\chi \in \Omega \setminus \{(7)\}}{arg \, min} \, \phi_{S}(\chi), \ \overline{\chi}_{S} = \underset{\chi \in \Omega \setminus \{(7)\}}{arg \, min} \, \phi_{S}(\chi; \beta = 0).$$

Clearly, $\phi_S(\chi_S') \leq \phi_S(\overline{\chi}_S)$, where the equality holds when $\overline{\chi}_S$ is an optimal solution to the calibrated model with $\beta \geq 0$ when relaxing the 1-neighbor constraint (7). Analogously, we let χ_R' and $\overline{\chi}_R$ denote the optimal solutions to the conservative-stochastic model under the estimated values for the adjustment factors and where all adjustment factors are set to zero, respectively, when relaxing the 1-neighbor constraint (7). Hence, similar to the stochastic model, for the conservative-stochastic model we have $\phi_{R_{0.05}}(\chi_R') \leq \phi_{R_{0.05}}(\overline{\chi}_R)$, where the equality holds when $\overline{\chi}_R$ is an optimal solution to the calibrated model with $\beta \geq 0$ when relaxing the 1-neighbor constraint (7). Consistent with our intuition, our numerical experiments show that $\overline{\chi}_S$ and $\overline{\chi}_R$ are indeed sub-optimal solutions to their corresponding stochastic and conservative-stochastic problems, respectively, when relaxing the 1-neighbor constraint, i.e., $\phi_S(\chi_S') < \phi_S(\overline{\chi}_S)$ and $\phi_{R_{0.05}}(\chi_R') < \phi_{R_{0.05}}(\overline{\chi}_R)$.

Table 2 summarizes the numerical analyses on characterizing the relationship between 1-neighbor constraint (7) and the runoff adjustment factor, β , at various levels of available budget. The second through fourth columns show the percentage reduction in total expected runoff volume under χ_S^{\star} , χ_S^{\prime} , and $\overline{\chi}_S$, respectively. The fifth through seventh columns show the percentage reduction in total expected runoff volume under χ_R^{\star} , χ_R^{\prime} , and $\overline{\chi}_R$, respectively. First note that, as discussed, the percentage reduction in total expected runoff volume under $\tilde{\chi}_S$ and $\tilde{\chi}_R$ are the same as those under χ_S^{\star} and χ_R^{\star} , respectively; hence, they are not included in the table. As seen in the table, the values under χ_S^\prime are larger than those obtained under χ_S^{\star} . Similarly, the values under χ_R' are larger than those obtained under χ_R^{\star} . This suggests that, as expected, the 1-neighbor constraint (7) is binding under the optimal solutions to both stochastic and conservative-stochastic models with the original feasible set Ω . In addition, as discussed, any difference between the values under χ_S' and $\overline{\chi}_S$, and those under χ_R' and $\overline{\chi}_R$ indicates that $\overline{\chi}_S$ and $\overline{\chi}_R$ are respectively sub-optimal solutions to the stochastic and conservative-stochastic models with the feasible set $\Omega\setminus\{(7)\}$. Accordingly, as seen in the table, $\overline{\chi}_S$ is sub-optimal at almost all budget levels, except 20 and 150 million dollars, in the stochastic model, and $\overline{\chi}_R$ is sub-optimal under available budgets of 25 and 50 million dollars in the conservative-stochastic model.

In summary, this analysis show that, given the structure of the underlying graph of sub-catchments $\mathbb{G}(V,A)$ in our study, 1-neighbor constraint (7) guarantees the optimality of a solution, regardless of accounting for adjustment factors. This has the potential to dramatically reduce the calibration efforts. However, note that using a set of well-estimated adjustment factors in models result in more accurate estimated values for the corresponding objective functions.

4.4. Incorporating sub-catchment-level runoff reduction considerations

In this section, we evaluate the impact of incorporating subcatchment-level runoff reduction considerations for certain subcatchments. Specifically, we focus on setting such constraints for sub-catchments with higher percentages of imperviousness. As discussed in Section 4.1 and Appendix F, regions 1 and 2 are the most populated sub-catchments in our watershed of interest, with the highest average percentages of impervious areas. Hence, for these regions we account for chance constraints, as discussed in Section 2.3, where we let $\gamma_t^i = 0.15$ under confidence level $(1 - \epsilon) = 0.95$. Based on our computational results, for any given subcatchment, the correlation between baseline surface runoff and the surface runoff after placing GI practice was not statistically significant (p-value < 0.05). Hence, we ignore the covariance terms in chance constraint (12).

Table 3Comparison of percentage reduction in total expected runoff under two-stage conservative-stochastic model, with and without chance constraints for the sub-catchments in regions 1 and 2. Note that $\gamma_i^t = 0.15$ and $1 - \epsilon = 0.95$.

Budget (million dollars)	Percent Reduction (Conservative-stochastic)	Percent Reduction (conservative-stochastic with chance constraints)	Relative Difference
10	5.30%	5.28%	0.38%
15	6.09%	6.09%	0.00%
20	6.87%	6.87%	0.00%
25	7.64%	7.61%	0.39%
50	10.97%	10.82%	1.37%
75	13.47%	13.19%	2.08%
100	14.86%	14.63%	1.55%
150	15.77%	15.58%	1.20%

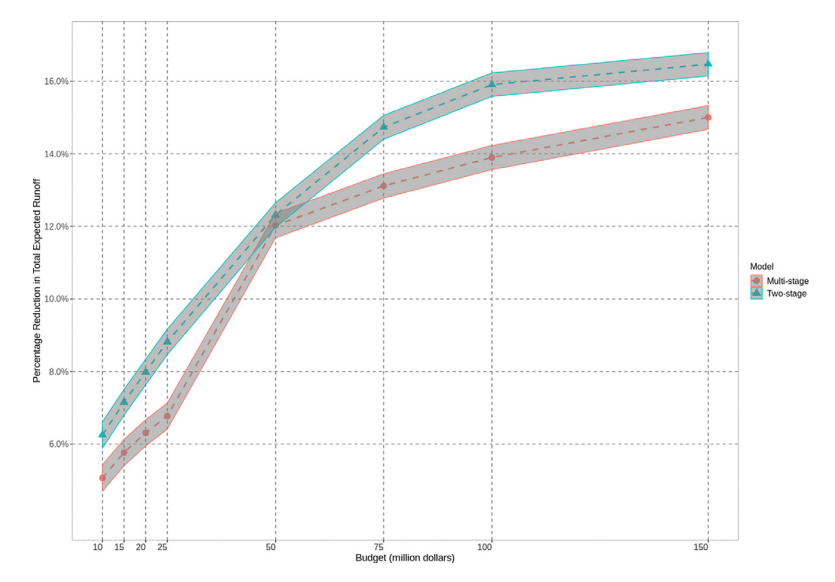


Fig. 11. Comparison of percentage reduction in total expected runoff under two-stage and multi-stage (three-stage) conservative-stochastic models, where the available budget ranges between 10 and 150 million dollars. The shaded areas represent the 95% CI for reduction in total expected runoff for the two models.

Table 3 summarizes the results of the two-stage conservative-stochastic models, with and with chance constraints for the sub-catchments in regions 1 and 2. As expected, the overall percentage reduction in total expected runoff is higher when not including the constraints, suggesting that the constraints are active in the optimal solution. It is worth noting that when the chance constraints are included, the density of the placed bioretention, of any size, in region 1 and 2 is higher than when these constraints are not included. In general, the observed relative difference in percentage runoff reduction is generally higher under higher available budget levels, with the highest relative difference in percentage runoff reduction observed under 75 million dollar budget, i.e., 2.08%.

4.5. Conservative-stochastic models: Two-stage vs multi-stage

In this section, we present and compare the computational results obtained from the two-stage and multi-stage conservative-stochastic models, under relaxed decision sets, i.e., we allow all GI types to be placed in any of the decision stages. Note that the projected total expected runoff volume for the multi-stage conservative-stochastic model is identical to that of two-stage conservative-stochastic model as reported in Section 4.2, i.e., for $\alpha=0.5$, the estimated 95% CI for the expected baseline surface runoff equals $4.56\times10^{11}\pm1.75\times10^{9}.$

Analogous to Figs. 10, 11 presents a comparison of percentage reduction in total expected runoff under two-stage and three-stage conservative-stochastic models, where the available budget ranges between 10 and 150 million dollars. First note that the results under this two-stage conservative-stochastic model are slightly better than those obtained from the two-stage conservative-stochastic

model reported in Section 4.2. This is mainly because in this section we relax the restrictions on decision sets, allowing all GI types to be placed in any of the stages. However, care needs to be taken when comparing the solutions across this section and Section 4.2, as in this section we use $\bar{T}=11$, whereas in Section 4.2 we had $\bar{T}=10$. The choice of $\bar{T}=11$ in this section is mainly to facilitate the comparison of two-stage and three-stage conservative-stochastic models, where in the latter model the 33-year planning horizon is divided into three 11-year periods, and GI placement occurs at the beginning of each period.

As seen in Fig. 11, the results of the two-stage conservative-stochastic outperforms that of three-stage conservative-stochastic under any given budget level. This partly stems from the fact that under our problem construction, as discussed in Section 2.2, the two-stage case is a relaxation of the multi-stage case. Lastly, as seen in the figure, the difference between the percentage reduction in total expected runoff under two-stage and multi-stage (three-stage) conservative-stochastic models is not constant across all budget levels. The lowest relative difference between the two percentage reductions is around 2.36%, occurring under 50 million dollars budget, whereas the highest difference between the two percentage reductions is 20.99%, occurring under 20 million dollars budget.

5. Summary and insights

Climate change threatens to overwhelm stromwater systems across the nation, rendering them ineffective. Green Infrastructure (GI) practices are low cost, low regret strategies that can contribute to urban runoff management. However, questions remain

10

as to how to best distribute GI practices through urban watersheds given precipitation uncertainty and hydrological responses to their installation. In this work, we showcase an approach that can enable city managers to incorporate the complexity and uncertainty of climate projections to make optimized choices for building resiliency into urban systems.

In this study, we developed stochastic programming models to determine the optimal placement of GI practices across a set of candidate locations in a watershed to minimize the total expected surface runoff under medium-term precipitation uncertainties, given an available budget. We proposed a novel scenario generation process that allowed us to efficiently evaluate the impact of precipitation on the entire watershed system under various combinations of GI practice placements. We calibrated the model using literature, historical precipitation data, future precipitation projections, and expert opinion and conducted a case study for an urban watershed in the City of Knoxville. We provided computational results and conducted extensive sensitivity analyses. Our results show that the optimal placement of GI practices within our watershed of interest can contribute to up to approximately 9.5% reduction in total expected runoff over the planning horizon, with a limited budget of 25 million

The reduction in total expected runoff obtained by the two modeling approaches are comparable. The two models, however, are quite different with respect to the computational time. That is, the computational time of the stochastic model is approximately two orders of magnitude larger than that of the conservative-stochastic model. This is mainly because of the lower number of scenarios used in the latter approach due to preprocessing of the precipitation projections, i.e., using Cls for the baseline runoff volume and surface runoff captured by a GI practice in any given sub-catchment, instead of all 100 scenarios per CGCM.

In our models, we accounted for hydrological connectivity in the watershed using an underlying acyclic connectivity graph of sub-catchments. Specifically, we introduced a 1-neighbor connectivity constraint over the graph to ensure that a large-scale GI practice can be placed in a given sub-catchment if there exists at least one large-scale GI practice in one of the subcatchments that are hydrologically connected to it. In addition, we carefully calibrated the runoff adjustments over pairs of hydrologically connected sub-catchments to more accurately estimate the impact of large-scale GI practices on runoff reduction not only within the sub-catchments in which they are placed, but also in their downstream sub-catchments. Our analysis shows that the 1-neighbor constraint protects the optimality of a solution in our watershed of interest, regardless of accounting for adjustment factors. This is mainly because of the particular structure of the connectivity graph of sub-catchments. More in-depth analysis is needed to establish sufficient conditions under which calibration of runoff adjustment factors is completely unnecessary.

To increase resilience against precipitation uncertainty, it is important to be able to minimize the expected total runoff volume across the entire watershed, while accounting for some level of confidence in runoff mitigation in certain (or all) sub-catchments. Hence, we introduced chance constraints that ensure the GI practices are placed across the watershed such that some level of confidence in the degree of runoff volume captured in given sub-

catchments are achieved. We provided the results for a case study using chance constraints, where we included constraints for the most populated sub-catchments, with the highest average percentages of impervious areas. We opted to include constraints for these sub-catchments as higher runoff in densely populated areas may result in significant water quality problems. It is important to note that including chance constraints would impose restrictions/prioritizations on placing GI practices across the watershed. Hence, the selection of candidate sub-catchments for imposing restrictions/prioritizations, and the degree of such restrictions/prioritizations, should be thoroughly studied and justified for any given watershed.

We also relaxed the restriction on decision sets, i.e., allowing for all GI types to be placed in any of the decision stages, in our conservative-stochastic model. As expected, we observed that relaxing the restriction on decision sets improves the solution. However, it is important to note that restricting when GI practices of certain types can be placed provides practical benefits regarding investment planning and managing the efforts required for implementing the different types of GI practices. For instance, considering that bioretentions are typically installed in relatively large, commercial scales and are held to high design standards, it may be more practical for city planners to allocate budget and/or land and negotiate contracts for their implementation during certain decision stages.

We also extended the two-stage conservative-stochastic model to multi-stage. Under our problem construction, we observed that the percent reduction in total expected runoff under two-stage case is greater than that under the multi-stage (three-stage) case.

In this study, we only accounted for two relatively similar types of GI practices, i.e., bioretentions and rain gardens. The selected types of GI practices are considered to be very efficient not only in reducing runoff volume, but also in treating stormwater quality. Note that the model developed is very versatile and allows for including more than two types of GI practices. Hence, accordingly, city planners can use the model using a wide array of GI practices to determine the best course of GI practice planning.

In this study, we accounted for future precipitation uncertainty using an array of CGCMs. This enabled us to account for climate change uncertainty when planning GI practices. Although we accounted for precipitation uncertainty, in this study we did not account for population growth and future urban development that can give rise to an increase in impervious area. Additional studies are needed to account for a close-loop system where a more livable city leads to urban population growth, which in turn leads to more runoff.

Lastly, in this study, we only accounted for runoff capturing properties of GI practices. As thoroughly discussed in the literature, GI practices provide a wide array of benefits, e.g., improving water and air quality, contributing to urban aesthetics, etc. Future multi-objective mathematical programs need to be developed to account for all benefits of GI practices when optimizing GI practice placement within an urban watershed.

Acknowlgedgments

This paper is based upon a research project supported by the National Science Foundation award number CMMI-1634975. We also acknowledge City of Knoxville–Stormwater Engineering Division for providing us the SWMM model of First Creek.

Appendix A. Notation

Table A.1

THE SELS.	
Set	Description
V	Set of sub-catchments
A	Set of sub-catchment connectivity arcs
G^I	Set of large-scale GI practices
G^{II}	Set of small-scale GI practices
$G=G^I\cup G^{II}$	Set of GI practices
L	Set of available levels of installation of GI practices
Ψ	Set of projected precipitation time series for the watershed, referred to as scenarios
$\hat{\Psi}$	Set of projected daily precipitation time series for the watershed, produced by the CGCMs

Table A.2 The parameters.

Parameter	Description
T	Length of the planning horizon in years
\overline{T}	The year in which a precipitation scenario is realized, referred to as time to realize a scenario
π^{ψ}	Probability of scenario $\psi\in\Psi$
$a_{i'i} \in A$	An arc indicating that the upstream sub-catchment $i' \in V$ is connected to the downstream sub-catchment $i \in V$
$Q_i^{\psi,t}$	Total baseline surface runoff under scenario $\psi \in \Psi$ over sub-catchment $i \in V$ in year $t \le T$ when no GI practice is placed
$2q_i^{\psi,t}(\alpha)$	The width of the 100(1- α)% CI for average baseline surface runoff volume within sub-catchment $i \in V$ under scenario $\psi \in \Psi$ in year $t \le T$
$Q_{i}^{\psi,t}$ $2q_{i}^{\psi,t}(\alpha)$ $\hat{Q}_{i,j,l}^{\psi,t}$	Surface runoff captured by GI practice of type $j \in G$ installed in level $l \in L$ within sub-catchment $i \in V$ under scenario $\psi \in \Psi$ in year $t \leq T$. We also define $\hat{Q}_{l,0,0}^{\psi,t} = 0$.
$2\hat{q}_{i,j,l}^{\psi,t}(\alpha)$	The width of the $100(1-\alpha)\%$ CI for the average surface runoff captured by GI practice of type $j \in G$ installed in level $l \in L$ within sub-catchment $i \in V$ under scenario $\psi \in \Psi$ in year $t \leq T$
$eta_{t',i',j',l'}^{t,i,j,l}$	Runoff 'adjustment factor' over the downstream sub-catchment $i \in V$, when a GI practice of type $j' \in G^l$ in level $l' \in L$ is placed within upstream sub-catchment $i' \in V$ and no GI practice or a GI practice of type $j \in G^l$ in level $l \in L$ is placed within the downstream sub-catchment $i \in V$
$C_{i,i}^t$	Per square feet present total cost of placing GI practice of type $j \in G$ within sub-catchment $i \in V$ in year $t \leq T$
$c_{i,i}^{t}$	Per square feet construction cost of a GI practice of type $j \in G$ in sub-catchment $i \in V$ in year $t \leq T$
$c_{i,i}^{t}$	Per square feet annual maintenance cost of a GI practice of type $j \in G$ in sub-catchment $i \in V$ in year $t \leq T$
r	Average annual inflation rate
$\delta_{i,i,l}$	Corresponding area (in square feet) of GI practice type $j \in G$ installed in level $l \in L$, within sub-catchment $i \in V$
η	Precipitation coefficient of variability

Table A.3 The Variables.

Variable	Description
$x_{i,j,l}^t$	First stage binary decision variable indicating whether or not a GI practice of type $j \in G^l \subset G$ in level $l \in L$ is placed within sub-catchment $i \in V$ in year $t \leq \overline{I} - 1$
$Z_{t,i,j,l}^{t',i',j',l'}$	First stage binary variable indicating whether or not GI practices of types j' , $j \in G^l$ in levels l' , $l \in L$ are placed within sub-catchment i' , $i \in V$ at times t' , $t \le T$, respectively. We also define $Z_{i,l,0,l}^{r',l',l',l'} = 0$.
$y_{i,j,l}^{\psi,t}$	Second stage binary decision variables indicating whether or not a GI practice of type $j \in G^{ll} \subset G$ in level $l \in L$ is placed within sub-catchment $i \in V$ year t , $\overline{T} \le t \le T$

Appendix B. Adjustment in surface runoff reduction due to GI placement in connected sub-catchments

Note that we assume 'adjustments' over downstream sub-catchments are additive. Hence, without loss of generality, here we simply present adjusting the runoff over the downstream sub-catchment i when a large-scale GI practice is placed within the single upstream sub-catchment $i' \in V$, $a_{i',i} \in A$.

Fig. B.1 presents the three cases to consider when accounting for surface run-off reduction over the downstream sub-catchment i due to placing a GI practice within the upstream sub-catchment i', $a_{i',i} \in A$, when accounting for large-scale practices only:

- (a) GI practice of type j' in level l' is placed within upstream sub-catchment i' in year t' after GI practice of type j in level l is placed within downstream sub-catchment i in year t such that $0 \le t \le t' \le \overline{T} 1$. In this case, run-off adjustment is needed only after the placement of a GI practice in the upstream sub-catchment i' in year t'. Hence the adjusted runoff reduction begins in year t';
- (b) GI practice of type j' in level l' is placed within upstream sub-catchment i' in year t' before GI practice of type j in level l is placed within downstream sub-catchment i in year t such that $0 \le t' \le t \le \overline{T} 1$. In this case, two levels of run-off adjustment are needed: The first adjustment is needed between years t' and t 1, and the second adjustment is needed on and after year t, i.e., after placing a GI practice in downstream sub-catchment i;
- (c) GI practice of type j' in level l' is placed within upstream sub-catchment i' in year t' and no GI placed in downstream sub-catchment i by the beginning of year \overline{T} , i.e., $0 \le t' \le \overline{T} 1$: In this case, run-off adjustment over downstream sub-catchment i is needed on and after year t'.

(c)
$$\downarrow \qquad \qquad \downarrow \qquad \qquad \qquad \qquad \qquad \downarrow \bar{T}-1$$

Fig. B.1. The three cases to consider when accounting for surface run-off reduction over a downstream sub-catchment due to a GI practice placement upstream, where the downstream and upstream sub-catchments are placed in years t and t', respectively. Attention is restricted to large-scale practices only.

First, consider the third term in the objective function (1), i.e.,

$$-\sum_{\{t'' \mid \max\{t \cdot \mathbb{1}_{\{j \neq 0\}}, t'\} \leq t'' \leq T\}} \beta_{i,j,l}^{i',j',l'} \left(Q_i^{\psi,t''} \left(x_{i',j',l'}^{t'} - z_{t,i,j,l}^{t',i',j',l'} \right) + \hat{Q}_{i,j,l}^{\psi,t''} \cdot z_{t,i,j,l}^{t',i',j',l'} \right). \tag{B.1}$$

Eq. (B.1) adjusts the run-off after placing a GI practice in the upstream sub-catchment i'. Also, consider the fourth term in the objective function (1), i.e.,

$$-\sum_{\{t''|t'\leq t''\leq t-1\}}\beta_{i,j,l}^{i',j',l'}\cdot Q_{i}^{\psi,t''}\cdot z_{t,i,j,l}^{t',i',j',l'}.$$
(B.2)

Eq. (B.2) adjusts the run-off after placing a GI practice in the upstream sub-catchment i' if it occurs before placing a GI practice in the downstream sub-catchment i.

In case (a), the runoff adjustment over downstream sub-catchment i for the years in which GI practices are placed in both sub-catchments i' and i, i.e., in year t'' such that $t' \le t'' \le T$ is given by Eq. (B.1), where the indicator function $\mathbb{1}_{\{j\neq 0\}}$ returns 1, and $\max\{t\cdot\mathbb{1}_{\{j\neq 0\}},t'\}$ returns t'. Note that $x_{[i',j',l'}^{t'}-z_{t,i,j,l}^{t',i',j',l'}=0$ since both $x_{[i',j',l']}^{t'}$ and $z_{t,i,j,l}^{t',i',j',l'}$ are equal to one. Therefore, in case (a) Eq. (B.1) simplifies as follows:

$$- \sum_{\{t'' \mid t' \leq t'' \leq T\}} \beta_{i,j,l}^{i',j',l'} \cdot \hat{Q}_{i,j,l}^{\psi,t''}.$$

Also, clearly, in case (a), Eq. (B.2) is not valid since $t \le t'$.

Similarly, for case (b), for the years in which GI practices are placed in both sub-catchments i' and i, i.e., in year t'' such that $t \le t'' \le T$, Eq. (B.1) simplifies as follows:

$$- \sum_{\{t'' \mid t \leq t'' \leq T\}} \beta_{i,j,l}^{i',j',l'} \cdot \hat{Q}_{i,j,l}^{\psi,t''}.$$

Also, for case (*b*), for the years in which the GI practice is placed in upstream sub-catchment i' and yet no GI is placed in downstream sub-catchment i, i.e., in year t'' such that $t' \le t'' \le t - 1$, Eq. (B.2) is active and simplifies as follows:

$$- \sum_{\{t'' \mid t' \leq t'' \leq t-1\}} \beta_{i,j,l}^{i',j',l'} \cdot Q_i^{\psi,t''},$$

because $z_{t,i,j,l}^{t',i',j',l'}$ equals one.

Lastly, for case (c), for the years in which the GI practice is placed in upstream sub-catchment i', i.e., in year t'' such that $t' \le t'' \le T$, the Eq. (B.1) simplifies as follows:

$$- \sum_{\{t'' \mid t' \leq t'' \leq T\}} \beta_{i,j,l}^{i',j',l'} \cdot \mathsf{Q}_i^{\psi,t''}.$$

The indicator function $\mathbb{1}_{\{j\neq 0\}}$ returns 0 and hence, $\max\{t \cdot \mathbb{1}_{\{j\neq 0\}}, t'\}$ returns t'. Note that variable $x_{i',j',l'}^{t'}$ is equal to one and variable $z_{i,i,l}^{t'}$ is equal to zero as j=0.

Also, note that Eq. (B.2) is equal to zero since variable $z_{t,i,i,l}^{t',i',j',l'}$ equals to zero in this case.

Appendix C. Multi-stage stochastic programming model for placing GI practices

Here we introduce the multi-stage stochastic programming approach. Let K denote the number of stages withing which we place GI of types G in the sub-catchments of interest. We let \overline{T}^K denote the time period of stage K where $0 < \overline{T}^1 < \cdots < \overline{T}^K < \overline{T}^{K+1} < \cdots < \overline{T}^K = T$. Accordingly, we let t^K denote a year during decision stage K, i.e. $\overline{T}^K \le t^K < \overline{T}^{K+1}$ under realization of random variable ψ . We let $\phi_{S_\alpha^K}(x,z)$

Please cite this article as: M. Barah, A. Khojandi and X. Li et al., Optimizing green infrastructure placement under precipitation uncertainty, Omega, https://doi.org/10.1016/j.omega.2020.102196

21

M. Barah, A. Khojandi and X. Li et al./Omega xxx (xxxx) xxx

denote the multi-stage conservative-stochastic model that denotes total expected surface runoff volume across the watershed of interest, which is given by

$$\min_{x,z} \phi_{S_{\alpha}}(x,z) = \mathbb{E}_{\psi_{\left[0,\overline{I}^{1}\right)}} \left[\min_{(x,z)} \phi_{S_{\alpha}^{1}}(x,z) + \dots + \mathbb{E}_{\psi_{\left[\overline{I}^{K-1},T\right)}} \left[\min_{(x,z)} \phi_{S_{\alpha}^{K}}(x,z) \right] \dots \right], \tag{C.3}$$

where $\mathbb{E}_{\psi_{[\overline{l}^{\kappa},\overline{l}^{\kappa+1})}}$ is the expectation of probability distribution of $\psi_{[\overline{l}^{\kappa},T)}$ in stage κ which also can be written as $\psi_{[\overline{l}^{\kappa},\overline{l}^{\kappa+1})}|\psi_{[\overline{l}^{\kappa-1},\overline{l}^{\kappa})}$. $\psi_{[\overline{l}^{\kappa-1},\overline{l}^{\kappa})}$. To simplify our multi-stage formulation, we assume stage-wise independence of probability distributions. That is, $\psi_{[\overline{l}^{\kappa},\overline{l}^{\kappa+1})}|\psi_{[\overline{l}^{\kappa-1},\overline{l}^{\kappa})}=\psi_{[\overline{l}^{\kappa},\overline{l}^{\kappa+1})}$. Hence, by swapping the min and expectation operators, we then have

$$\min_{x,z} \phi_{S_{\alpha}}(x,z) = \min_{(x,z)} \mathbb{E}_{\psi_{[0,T)}} \Big[\phi_{S_{\alpha}^{1}}(x,z) + \dots + \phi_{S_{\alpha}^{K}}(x,z) \dots \Big], \tag{C.4}$$

Also, consistent with our extended two-stage formulation, we assume there exists a discrete support for the probability distribution of $\psi_{[\overline{I}^{\kappa},\overline{I}^{\kappa+1})}$, denoted by the set $\{\psi^1_{[\overline{I}^{\kappa},\overline{I}^{\kappa+1})}:\pi^{\psi^1},\cdots,\psi^{|\Psi|}_{[\overline{I}^{\kappa},\overline{I}^{\kappa+1})}:\pi^{\psi^{|\Psi|}}\}$ in which π^{ψ} is the probability of each discrete support member $(\sum_{\psi\in\Psi}\pi^{\psi}=1)$. Hence, we let $x^{\psi,t}_{i,j,l}$ be a binary variable denoting if GI of type j with size i is placed in sub-catchment i under scenario ψ , $\psi\in\Psi^{\kappa}$. Also, we let $x^{\psi,t}_{i,j,l}$ be binary variable alias to $x^{\psi,t}_{i,j,l}$. Regarding the interaction between sub-catchments, we let $z^{\psi,t',i',j',l'}_{t,i,j,l}$ denote the binary variable indicating whether GI practices of types j', $j\in G^I$ in levels l', $l\in L$ are installed within sub-catchment i', $i\in V$ in years $T^{\kappa-1}\leq t',t< T^{\kappa}$ under scenario ψ , respectively. Therefore, the extended formulation of $\mathbb{E}_{\psi_{[\overline{I}^{\kappa-1},T)}}$ $[\min_{(x,z)\in\Omega}\phi_{S^{\kappa}_{i}}(x,z)]$ is given by

$$\begin{split} &\mathbb{E}_{\psi_{\mid \overline{I}^{K-1}, T \rangle}} \left[\min_{(x,z) \in \Omega} \phi_{S_{K}^{K}}(x, z) \right] \\ &= \sum_{\psi \in \Psi^{K}} \pi^{\psi} \cdot \left[\sum_{i \in V} \sum_{\{t \mid \overline{I}^{K-1} \leq t \leq T \}} Q_{i}^{\psi, t} + q_{i}^{\psi, t}(\alpha) \right. \\ &- \sum_{i \in V} \sum_{j \in G} \sum_{l \in I} \sum_{\{t \mid T^{K-1} \leq t^{K-1} \leq T-1 \}} \sum_{\{t' \mid T^{K-1} \leq t' \leq T \}} \left(\hat{Q}_{i, j, l}^{\psi, t'} - \hat{q}_{i, j, l}^{\psi, t'}(\alpha) \right) \cdot x_{i, j, l}^{\psi, t} \\ &- \sum_{a_{l', i} \in A} \sum_{j \in C^{l} \cup \{0\}} \sum_{j' \in C^{l}} \sum_{l \in L} \sum_{l' \in L} \sum_{\{t \mid T^{K-1} \leq t' \leq T \}} \sum_{\{t' \mid T^{K-1} \leq t' \leq T \}} \sum_{\{t'' \mid \max_{l \in L} \{t, T^{K-1} \leq t' \leq T \}} \sum_{t'' \in T^{l}, j, l'} \\ &\times \beta_{i, j, l}^{\ell', j', l'} \left(\left(Q_{i, j'}^{\psi, t''} - q_{i}^{\psi, t''}(\alpha) \right) \left(x_{i', j', l'}^{\psi, t'} - z_{t, i, j, l}^{t', l', l', l'} \right) \right. \\ &+ \left. \left(\hat{Q}_{i, j, l}^{\psi, t''} - \hat{q}_{i, j, l}^{\psi, t''}(\alpha) \right) \cdot z_{t, i, j, l}^{\psi, t', t', j', l', l'} \right) \\ &- \sum_{a_{l', i} \in A} \sum_{j \in C^{l} \cup \{0\}} \sum_{j' \in C^{l}} \sum_{l \in L} \sum_{l' \in L} \sum_{\{t \mid T^{K-1} \leq t' \leq t-1 \}} \sum_{\{t'' \mid T^{K-1} \leq t' \leq t-1 \}} \sum_{\{t'' \mid t'' \leq t'' \leq t-1 \}} \sum_{\{t'' \mid t'' \leq t'' \leq t-1 \}} \sum_{\{t'' \mid t'' \leq t'' \leq t-1 \}} \left. \beta_{i, j, l}^{\ell', j', l'} - q_{i, l''}^{\psi, t''}(\alpha) \right) \cdot z_{t, i, j, l}^{\psi, t', l', j', l'} \right]. \end{split}$$

$$\text{s.t. } \sum_{i \in V} \sum_{l \in I} \sum_{l \in I} \sum_{t \in T^{K-1} \neq t \in T^1} C^t_{i,j} \cdot \delta_{i,j,l} \cdot \left(x^{\psi,t}_{i,j,l} - x'^{\psi,t}_{i,j,l} \right) \leq B^{\Psi^K}, \qquad \forall \psi \in \Psi^K, \tag{C.6}$$

$$\forall \psi \in \Psi^{K}, \forall i', i \in V, \\ a_{i',i} \in A, \\ \forall j', j \in G^{I}, \forall \underline{l'}, l \in L,$$
 (C.7)

$$x_{i,j,l}^{\psi,t} \geq \sum_{j' \in G^{l}} \sum_{l' \in L} \sum_{\{t' \mid T^{K-1} \leq t' \leq T\}} z_{t,i,j,l}^{\psi,t',i',j',l'}, \qquad \begin{aligned} \forall \psi \in \Psi^{K}, \forall i, i' \in V, \\ a_{i',i} \in A, \\ \forall j \in G^{l}, \forall l \in L, \\ T^{K-1} \leq t \leq T, \end{aligned}$$

$$(C.8)$$

 $0 < t', t \leq \overline{T} - 1,$

$$x_{i',j',l'}^{\psi,t'} \ge \sum_{j \in G^{l}} \sum_{l \in L} \sum_{\{t \mid T^{K-1} \le t \le T\}} z_{t,i,j,l}^{\psi,t',i',j',l'}, \qquad \begin{cases} \forall \psi \in \Psi^{K}, \forall i, i' \in V, \\ a_{i',i} \in A, \\ \forall j' \in G^{l}, \forall l' \in L, \\ T^{K-1} \le t' \le T, \end{cases}$$
(C.9)

$$\forall \psi \in \Psi^{K},
\forall i', i \in V, a_{i',i} \in A,
j = 0, \forall j' \in G^{I},
\forall l, l' \in L,
T^{K-1} < t, t' < T.$$
(C.10)

 $z_{t,i,i,l}^{\psi,t',i',j',l'}=0,$

22

Please cite this article as: M. Barah, A. Khojandi and X. Li et al., Optimizing green infrastructure placement under precipitation uncertainty, Omega, https://doi.org/10.1016/j.omega.2020.102196

M. Barah, A. Khojandi and X. Li et al./Omega xxx (xxxx) xxx

$$\sum_{j \in C^l} \sum_{l \in L} \sum_{\{t \mid T^{K-1} \leq t \leq T\}} X^t_{i,j,l} \leq \sum_{a_{i',j} \in A} \sum_{j \in C^l} \sum_{l \in L} \sum_{\{t \mid T^{K-1} \leq t \leq T\}}$$

$$\sum_{j \in G'} \sum_{l \in L} \sum_{\{t \mid T^{K-1} \le t \le T\}} x_{i,j,l}^{\psi,t} \le 1,$$

$$x_{i,j,l}^{\psi,t} - x_{i,j,l}^{\psi',t'} \ge 0,$$

$$2x'_{i,j,l}^{\psi,t} - x_{i,j,l}^{\psi,t} - x_{i,j,l}^{\psi',t'} \ge 0,$$

$$x_{i,j,l}^{\psi',t'} - {x'}_{i,j,l}^{\psi,t} \geq 0,$$

$$x_{i,j,l}^{\psi,t}, z_{t,i,j'',l}^{\psi,t',i',j',l'} \in \{0,1\},$$

$$x_{i',j,l}^{\psi,t}, \forall i \in V, \tag{C.11}$$

$$\forall \psi \in \Psi^K, \forall i \in V, \tag{C.12}$$

$$\begin{array}{l} \forall \psi \in \Psi^{K}, \forall \psi' \in \Psi^{K-1}, \\ \Psi^{K} \text{ sub-tree } \Psi^{K-1} \\ \forall i \in V, \forall j \in G, \forall l \in L, \\ \overline{T}^{K-1} \leq t \leq T, \\ \overline{T}^{K-2} \leq t' < \overline{T}^{K-1}, \end{array} \tag{C.13}$$

$$\begin{aligned} \forall \psi \in \Psi^{K}, \forall \psi' \in \Psi^{K-1}, \\ \Psi^{K} \text{ sub-tree } \Psi^{K-1} \\ \forall i \in V, \forall j \in G, \forall l \in L, \\ \overline{T}^{K-1} &\leq t \leq T, \\ \overline{T}^{K-2} &\leq t' < \overline{T}^{K-1}, \end{aligned} \tag{C.14}$$

$$\begin{aligned} \forall \psi \in \Psi^{K}, \forall \psi' \in \Psi^{K-1}, \\ \Psi^{K} \text{ sub-tree } \Psi^{K-1} \\ \forall i \in V, \forall j \in G, \forall l \in L, \\ \overline{T}^{K-1} \leq t \leq T, \\ \overline{T}^{K-2} \leq t' < \overline{T}^{K-1}, \end{aligned} \tag{C.15}$$

$$\forall i', i \in V, a_{i',i} \in A,$$

$$\forall j \in G, \forall j', j'' \in G^{l},$$

$$\forall l', l \in L, \forall \psi \in \Psi,$$

$$T^{K-1} \leq t, t' \leq T.$$
(C.16)

where B^{Ψ^K} , denotes the remaining of total allocated budget, given the placed GI practices in parent nodes of Ψ^K , i.e., stages 0 to K-1. The objective function (C.5) minimizes the total expected surface runoff volume in stage K. Definitions of constraints (C.6)–(C.12) are similar to counterpart constraints defined in Ω . Equations defined in (C.13) is *non-anticipativity* constraints for multi-stage stochastic programming. That is, a decision made on a node in the scenario tree is sustained in its sub-trees. We set constraints (C.14) and (C.15) to ensue that cost of GI practices that are already placed on a node under a scenario, would not be double counted in the sub-tree of the scenario. Lastly, constraint (C.16) maintains the binary conditions of the decision variables.

Appendix D. Coupled Global Circulation Models (CGCMs)

Table D.1Ten coupled global circulation models used for projecting future precipitation.

Model Name	Institution
ACCESS: The Australian Community Climate and Earth-System Simulator [1] BCC-CSM: Beijing Climate Center Climate System Model [2], referred to as 'BCC' in the text	Commonwealth Scientific and Industrial Research Organisation Beijing Climate Center, China Meteorological Administration
CCSM4: The NCAR's Community Climate System Model [3]	Climate and Global Dynamics Laboratory (CGD) at the National Center for Atmospheric Research (NCAR)
CMCC-CM : The Centro Euro-Mediterraneo sui Cambiamenti Climatici Climate Model [4], referred to as 'CMCC' in the text	Euro-Mediterranean Center on Climate Change
FGOALS: Flexible Global Ocean Atmosphere Land System [7]	Institute of Atmospheric Physics, Chinese Academy of Sciences, State Key Laboratory of Numerical Modeling for Atmospheric Sciences and Geophysical Fluid Dynamics
GFDL-ESM2M: Geophysical Fluid Dynamics Laboratory Earth System Model [8], referred to as 'GFDL' in the text	Geophysical Fluid Dynamics Laboratory (Princeton University)
IPSL-CM5A: The Institut Pierre Simon Laplace Climate Model [10], referred to as 'IPSL' in the text	Institut Pierre Simon Laplace
MPI-ESM-MR: Max-Planck-Institute Earth System Model Mixed Resolution [11], referred to as 'MPI' in the text	Max Planck Institute for Meteorology
MRI-CGCM3: Japanese Meteorological Research Institute Coupled Global Climate Model [12], referred to as 'MRI' in the text	Meteorological Research Institute (MRI) of the Japan Meteorological Agency
NorESM1-M: Norwegian Earth System Model [16], referred to as 'NorESM' in the text	Multi-institutional, coordinated climate research in Norway

Please cite this article as: M. Barah, A. Khojandi and X. Li et al., Optimizing green infrastructure placement under precipitation uncertainty, Omega, https://doi.org/10.1016/j.omega.2020.102196

Table E.1Summary characteristics of the 140 sub-catchments within our watershed of interest, categorized by percent of imperviousness, percent of slope, and Manning's n for overland flow over the pervious portion of the sub-catchment.

% of Imp.	% of Slope	Manning's n	Number of Sub-catchments	Average Area (acres)	Average Imp. (%)	Average Slope (%)	Average Manning's n
low	low	med	2	117.95	7.85	1.56	0.248
low	low	high	9	153.24	4.64	1.68	0.281
low	med	high	8	139.16	3.94	2.86	0.290
low	high	high	16	98.50	4.78	6.59	0.282
med	low	med	2	92.14	11.60	1.46	0.250
med	low	high	2	80.65	8.80	1.86	0.262
med	med	med	3	154.36	10.43	2.74	0.255
med	med	high	9	76.10	9.69	2.75	0.272
med	high	med	5	85.88	10.62	7.29	0.248
med	high	high	13	90.97	9.47	8.27	0.266
high	low	low	8	66.28	20.53	1.58	0.211
high	low	med	7	139.53	16.57	1.58	0.247
high	low	high	5	147.74	16.62	1.78	0.283
high	med	low	10	88.49	23.39	3.02	0.219
high	med	med	3	43.49	18.93	2.46	0.247
high	med	high	2	121.45	23.15	3.15	0.283
high	high	low	18	67.87	19.82	5.11	0.211
high	high	med	12	90.44	14.36	6.70	0.247
high	high	high	6	121.26	17.87	6.09	0.282

Appendix E. Calculating runoff adjustment factor over a downstream sub-catchment

We designed a set of experiments to calculate runoff adjustment factor over a downstream sub-catchment for any given pair of hydrologically connected sub-catchments. Consistent with the literature [24], we only use the most significant sub-catchment characteristics related to surface runoff in our experiments, namely, sub-catchments' percent of imperviousness, percent of slope, and Manning's n for overland flow over the pervious portion of the sub-catchment. Next, we use the values of these characteristics for the sub-catchments in the watershed of interest and calculate their corresponding quartiles. Accordingly, we stratify each characteristic into three categories of low, medium, and high, if the corresponding value is at or below the first quartile, between first and third quartiles, and above the third quartile. Table E.1 summarizes the combination of categories along with the number of observed sub-catchments within each one for our watershed of interest.

Consequently, we execute the SWMM model for all pairs of sub-catchments, given the average values for the categories in our watershed of interest. We run these simulations under the randomly selected precipitation events in the 'SWMM Simulation' step of the procedure described in Section 3.3. The runoff adjustment factor over a downstream sub-catchment is then estimated as the average difference in runoff coefficient in the sub-catchment over all precipitation events when a certain GI practice is placed within the upstream sub-catchment and no GI is placed there (i.e., no treatment). Fig. E.1 presents the heat map of runoff adjustment factors over the downstream sub-catchment, given all observed combinations of sub-catchment characteristics' categories in the watershed of interest.

Appendix F. Summary of the characteristics of the sub-catchments in first creek, Knoxville, TN

Table F.1Summary of the characteristics of the sub-catchments in First Creek as labeled in Fig. F.1.

Region	Total Area (Acres)	Average Impervious Area (%)	Average slope (%)
1	1292.05	23.36	3.65
2	3187.31	18.01	4.74
3	4915.84	8.07	3.83
4	807.43	8.31	6.12
5	3745.82	12.61	4.31

Appendix G. Sensitivity analyses

In this section, we examine the sensitivity of the solutions with respect to some of the important calibrated parameters, including the years to realize a scenario, \overline{T} , the ratio of maintenance cost to construction cost, ρ , and the runoff adjustment factor, $\beta_{i,j,l}^{i',j',l'}$. In all cases, we conduct the sensitivity analysis under a wide range of available budgets.

First, we perform sensitivity analysis on the years to realize a scenario, \overline{T} , under different budget limitations. Fig. G.1 shows the percentage reduction in total expected runoff for $\overline{T}=5$, 10, and 15, with the total available budget ranging between 10 and 150 million dollars. As seen in the figure, realizing a scenario sooner, i.e., smaller values of \overline{T} , results in a larger reduction in total expected runoff. However, the differences among the percentage runoff reductions for the three cases is low, and decreases in the amount of available budget. For instance, given 10 million dollars available budget, the maximum difference among the percentage runoff reductions equals 1.00% and 0.85% for the stochastic and conservative-stochastic models, respectively. This maximum difference decreases to almost zero for budgets larger than 50 million dollars for both models. This is mainly because under a large enough available budget, large-scale bioretentions are

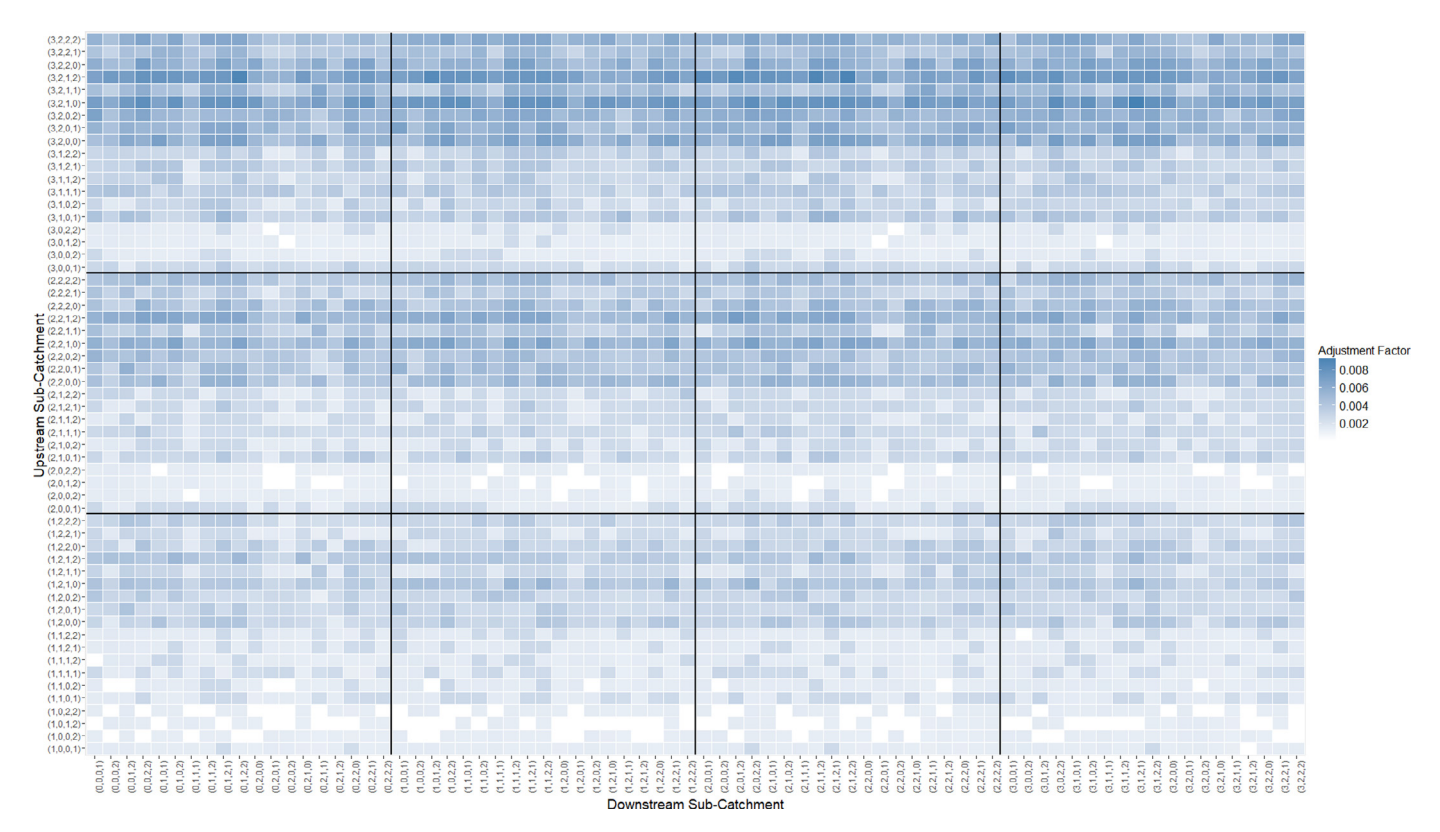


Fig. E.1. Heat map of the runoff adjustment factors over the downstream sub-catchment, given all observed combinations of sub-catchment characteristics' categories in the watershed of interest. Sub-catchment characteristics are shown as tuples, where the first element corresponds to the GI level – 0 encodes no treatment and 1–3 refer to the levels low, medium, and large bioretentions, respectively. Elements 2–4 of the tuple correspond to percent of imperviousness, percent of slope, and Manning's n for overland flow over the pervious portion of the sub-catchment, each of which are categorized into three levels of 0–2, encoding low, medium, and high, respectively.

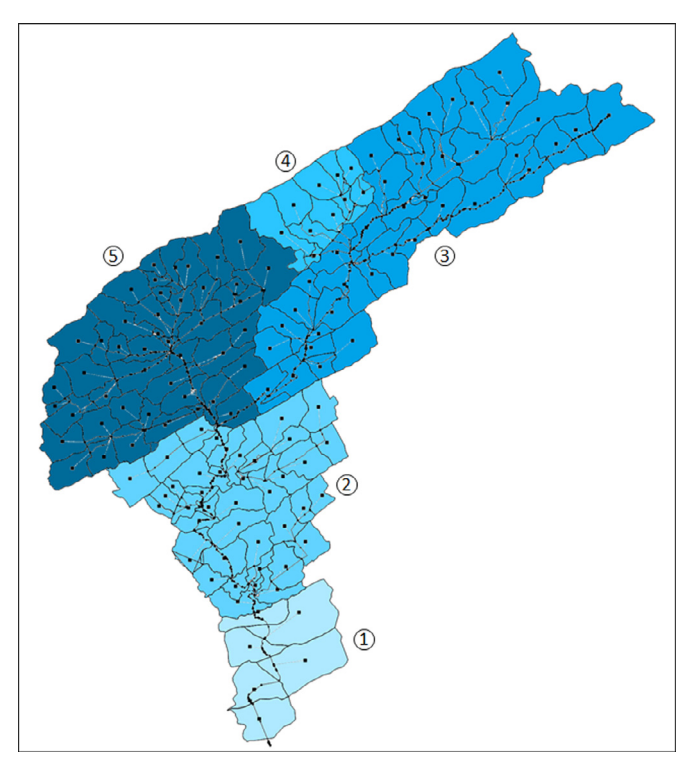


Fig. F.1. Watershed of First Creek, grouped based on similarities in sub-catchment characteristics.

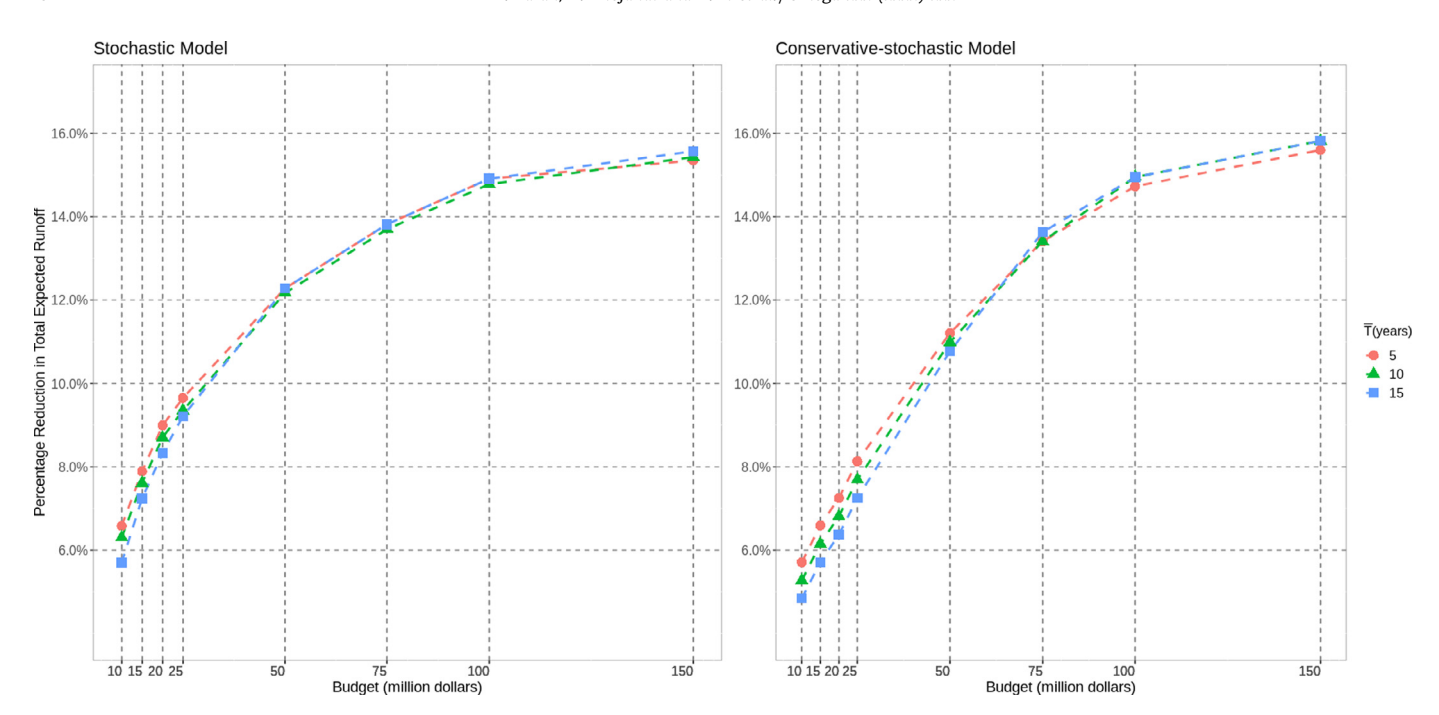


Fig. G.1. Percentage reduction in total expected runoff for $\overline{T} = 5$, 10, and 15 years, where the available budget ranges between 10 and 150 million dollars.

Table G.1Percentage reduction in total expected runoff for different ratios of maintenance cost to construction cost, ρ , where the available budget ranges between 10 and 150 million dollars.

Budget (million dollars)	Ratio of ma	intenance cost to	construction cos	st, p				
	Stochastic N	/lodel		conservative-stochastic Model				
	1%	3%	6%	10%	1%	3%	6%	10%
10	6.26%	6.22%	6.16%	6.09%	5.32%	5.30%	5.27%	5.23%
15	7.59%	7.55%	7.50%	7.43%	6.12%	6.09%	6.05%	6.00%
20	8.61%	8.56%	8.51%	8.44%	6.90%	6.87%	6.81%	6.75%
25	9.36%	9.33%	9.26%	9.20%	7.68%	7.64%	7.58%	7.49%
50	12.18%	12.14%	12.07%	11.98%	11.04%	10.97%	10.88%	10.76%
75	13.75%	13.71%	13.65%	13.58%	13.52%	13.47%	13.37%	13.25%
100	14.78%	14.74%	14.69%	14.62%	14.90%	14.86%	14.79%	14.70%
150	15.37%	15.37%	15.37%	15.37%	15.77%	15.77%	15.77%	15.77%

Table G.2Percentage reduction in total expected runoff under different levels of runoff adjustment factors, where the available budget ranges between 10 and 150 million dollars.

Budget (million dollars)	Levels of Runoff Adjustment Factor								
	Stochastic	Model		conservative-stochastic Model					
	No Adj.	-50%	Estimated Adj.	50%	No Adj.	-50%	Estimated Adj.	50%	
10	6.16%	6.19%	6.22%	6.25%	5.25%	5.28%	5.30%	5.32%	
15	7.46%	7.50%	7.55%	7.60%	6.03%	6.06%	6.09%	6.12%	
20	8.46%	8.51%	8.56%	8.62%	6.78%	6.83%	6.87%	6.92%	
25	9.21%	9.26%	9.33%	9.39%	7.53%	7.59%	7.64%	7.70%	
50	11.99%	12.07%	12.14%	12.22%	10.78%	10.88%	10.97%	11.07%	
75	13.57%	13.64%	13.71%	13.78%	13.20%	13.33%	13.47%	13.60%	
100	14.58%	14.66%	14.74%	14.83%	14.64%	14.74%	14.86%	14.97%	
150	15.22%	15.30%	15.37%	15.45%	15.60%	15.69%	15.77%	15.85%	

placed within almost all sub-catchments in the first stage. Therefore, because at most one type of GI practice can be placed within any given sub-catchment, there would be few vacant sub-catchments in which rain gardens can be placed after realizing a scenario at time \overline{T} in the second stage. This, in turn, decreases the impact of second stage decisions, resulting in almost no significant difference between the three cases under larger amounts of budget.

Next, we conduct sensitivity analysis on the amount of maintenance cost. As discussed in Section 3.1, we set the annual annual GI maintenance cost equal to 3% of its construction cost, i.e., $\rho = 3\%$. Table G.1 presents the percentage reduction in total expected runoff under different ratios of maintenance cost to construction cost, ρ , ranging between 1% and 10%, where the available budget ranges between 10 and 150 million dollars. In general, as expected, given any available budget, the percentage runoff reduction non-increases in ρ . This

M. Barah, A. Khojandi and X. Li et al./Omega xxx (xxxx) xxx

is because as ρ increases, a larger portion of the budget must be allocated to maintain the GI practices to be placed. For instance, under 10 million dollars available budget, in the stochastic model, the runoff reduction decreases by 0.13% when ρ increases from 3% to 10%. Similarly, in the conservative-stochastic model, the corresponding runoff reduction decrease equals to 0.07%. Note that for large amounts of available budget, i.e., under 150 million dollars available budget, changing ρ no longer impacts the solution as the available budget is high enough that covers all construction and maintenance costs.

Finally, we conduct sensitivity analysis with respect to the value of runoff adjustment factor, $\beta_{i,j,l}^{i',j',l'}$. Table G.2 presents the percentage reduction in total expected runoff under the estimated adjustment factors, no adjustment, and where the estimated adjustment is modified by 50%, where the available budget ranges between 10 and 150 million dollars. As seen in the table, connectivity, captured through adjustment factors, contributes to up to 0.16% and 0.27% reduction in total runoff under various available budgets for the stochastic and conservative-stochastic models, respectively. Also, note that connectivity contributes to a higher percentage of runoff reduction under higher levels of available budget. This is mainly because in such cases, a larger number of bioretentions are placed across the watershed, which potentially results in a higher number of pairs of hydrologically connected sub-catchments.

Supplementary material

Supplementary material associated with this article can be found, in the online version, at doi:10.1016/j.omega.2020.102196.

References

- [1] Commonwealth Scientific and Industrial Research Organisation; 2016. [Last accessed on September 10, 2016]. http://www.csiro.au/en/Research/OandA/Areas/Assessing-our-climate/CAWCR/ACCESS/.
- [2] Beijing Climate Center, China Meteorological Administration; 2014. [Last accessed on September 10, 2016]. http://forecast.bcccsm.cma.gov.cn/htm/.
- [3] Climate and Global Dynamics Laboratory (CGD) at the National Center for Atmospheric Research (NCAR); 2016. [Last accessed on September 10, 2016]. http://www.cesm.ucar.edu/models/ccsm4.0//.
- [4] Euro-Mediterranean Center on Climate Change; 2016. [Last accessed on September 10, 2016]; http://www.cmcc.it/models/cmcc-cm.
- [5] United States Environmental Protection Agency (EPA). Green Infrastructure Website; 2016. [Last accessed on February 11, 2016]. http://water.epa.gov/infrastructure/greeninfrastructure/.
- [6] United States Environmental Protection Agency (EPA). Operation and Maintenance Considerations for Green Infrastructure; 2018. [Last accessed on July 31, 2018]. https://www.epa.gov/G3/operation-and-maintenance-considerations-green-infrastructure.
- [7] Institute of Atmospheric Physics, Chinese Academy of Sciences, State Key Laboratory of Numerical Modeling for Atmospheric Sciences and Geophysical Fluid Dynamics; 2013. [Last accessed on September 10, 2016]. http://www.lasg.ac.cn/.
- [8] Geophysical Fluid Dynamics Laboratory (Princeton University); 2012. [Last accessed on September 10, 2016]. https://www.gfdl.noaa.gov/earth-system-model/.
- [9] Green infrastructure types; 2017. [Last accessed on July 31, 2018]. http://www.greenbelt.ca/gi_rain_garden_and_bioretention.
- [10] Institut Pierre Simon Laplace; 2016. [Last accessed on September 10, 2016]. http://icmc.ipsl.fr/.
- [11] Max Planck Institute for Meteorology. 2013. [Last accessed on September 10, 2016]; http://www.mpimet.mpg.de/en/science/models/mpi-esm.html.
- [12] Meteorological Research Institute (MRI) of the Japan Meteorological Agency; 2012.[Last accessed on September 10, 2016]. http://ds.data.jma.go.jp/tcc/tcc/products/gwp/gwp7/html_e/model.html.
- [13] National Association of City Transportation Officials. 2017. [Last accessed on November 19, 2018]; https://nacto.org/.
- [14] Bioretention cell sizing; 2017. [Last accessed on November 19, 2018]. https://nacto.org/publication/urban-street-stormwater-guide/stormwater-elements/bioretention-cell-sizing/.
- [15] National Centers for Environmental Information (NCEI); 2016. [Last accessed on July 31, 2018]. https://www.ncdc.noaa.gov/.
- [16] Multi-institutional, Coordinated Climate Research in Norway; 2013. [Last accessed on September 10, 2016]. http://folk.uib.no/ngfhd/EarthClim/.
- [17] Tennessee Stormwater Training; 2015. [Last accessed on October 22, 2018]. https://tnpermanentstormwater.org/manual.asp.
- [18] Current US inflation rates; 2018. [Last accessed on July 31, 2018]. https://www.usinflationcalculator.com/inflation/current-inflation-rates/.
- [19] EPA issues guidance for cities on managing sewer overflows with green infrastructure. 2014. Bloomberg News Report issued on [March 10, 2014].
- [20] Bonnin GM, Martin D, Lin B, Parzybok T, Yekta M, Riley D. Precipitation-frequency atlas of the United States. NOAA Atlas 2006;14(2).
- [21] Cambez M, Pinho J, David L. Using SWMM 5 in the continuous modelling of stormwater hydraulics and quality. In: Proceedings of the 11th international conference on urban drainage, Edinburgh, Scotland, UK; 2008.
- [22] Catalano de Sousa MR, Montalto FA, Gurian P. Evaluating green infrastructure stormwater capture performance under extreme precipitation. J. Extreme Events 2016;3(02):1650006.
- [23] Chang C-C, Digiovanni K, Zhang G, Yang X, You S-H. Sustainability. Water Environ Res 2015;87(10):1208–55.
- [24] Choi K-s, Ball JE. Parameter estimation for urban runoff modelling. Urban Water 2002;4(1):31-41.
- [25] Daniels T. Environmental planning handbook, Routledge; 2017.
- [26] Davis AP, Hunt WF, Traver RG, Clar M. Bioretention technology: overview of current practice and future needs. J Environ Eng 2009;135(3):109-17.
- [27] De Luis M, González-Hidalgo J, Raventós J, Sánchez J, Cortina J. Distribución espacial de la concentración y agresividad de la lluvia en el territorio de la comunidad valenciana. Cuaternario y Geomorfología 1997;11(3-4):33-44.
- [28] Dietrich A, Yarlagadda R, Gruden C. Estimating the potential benefits of green stormwater infrastructure on developed sites using hydrologic model simulation. Environ Progr Sustain Energy 2017;36(2):557–64.
- [29] Doan LN, Davis AP. Bioretention-cistern-irrigation treatment train to minimize stormwater runoff. J Sustain Water Built Environ 2017;3(2):04017003.
- [30] Echols S, Pennypacker E. Artful rainwater design: creative ways to manage stormwater. Island Press; 2015.
- [31] Efron B. Bootstrap methods: another look at the jackknife. In: Breakthroughs in statistics. Springer; 1992. p. 569-93.
- [32] (EPA) E.P.A., 2016, Opti-tool: Epa region 1's stormwater management optimization tool. [Last accessed on June 22, 2018]. https://www.epa.gov/tmdl/opti-tool-epa-region-1s-stormwater-management-optimization-tool.
- [33] Epps T, Hathaway JM. Using spatially-identified effective impervious area to target green infrastructure retrofits: A modeling study in knoxville, TN. J Hydrol 2018;575:442–53.
- [34] Epps T, Hathaway JM. Establishing a framework for the spatial identification of effective impervious areas in gauged basins: review and case study. J Sustain Water Built Environ 2018;4(2):05018001.
- [35] TexasAgriLife AE. Rain gardens for stormwater management. Texas A& M University; 2012.
- [36] Federal Emergency Management Agency (FEMA). Flood insurance study, Knox County, Tennessee, and incorporated areas. United States Department of Homeland Security: 2013.
- [37] Field CB. Managing the risks of extreme events and disasters to advance climate change adaptation: special report of the intergovernmental panel on climate change. Cambridge University Press; 2012.
- [38] Golden HE, Hoghooghi N. Green infrastructure and its catchment-scale effects: an emerging science. Wiley Interdisc Rev Water 2018;5(1):e1254.
- [39] Guo JC, Urbonas B. Volume-based runoff coefficients for urban catchments. J Irrig Drain Eng 2013;140(2):04013013.
- [40] Hoffman FM, Hargrove Jr WW, Erickson III DJ, Oglesby RJ. Using clustered climate regimes to analyze and compare predictions from fully coupled general circulation models. Earth Interact 2005;9(10):1–27.
- [41] Homer C, Dewitz J, Yang L, Jin S, Danielson P, Xian G, et al. Completion of the 2011 national land cover database for the conterminous united states–representing a decade of land cover change information. Photogram Eng Remote Sens 2015;81(5):345–54.
- [42] Huff FA. Time distribution of rainfall in heavy storms. Water Resour Res 1967;3(4):1007–19.
- [43] Jang S, Cho M, Yoon J, Yoon Y, Kim S, Kim G, et al. Using SWMM as a tool for hydrologic impact assessment. Desalination 2007;212(1-3):344-56.

Please cite this article as: M. Barah, A. Khojandi and X. Li et al., Optimizing green infrastructure placement under precipitation uncertainty, Omega, https://doi.org/10.1016/j.omega.2020.102196

27

JID: OME m5G;February 11, 2020;22:18

M. Barah, A. Khojandi and X. Li et al./Omega xxx (xxxx) xxx

[44] Jarden KM, Jefferson AJ, Grieser JM. Assessing the effects of catchment-scale urban green infrastructure retrofits on hydrograph characteristics. Hydrol Process 2016:30(10):1536-50

- [45] Junker W., Flash flooding: a lesser known, but leading weather killer. The Washington Post; 2013. Last accessed on February 14, 2016 https://www.washingtonpost.com/ /news/capital-weather-gang/wp/2013/07/11/flash-flooding-a-lesser-known-but-leading-weather-killer
- [46] Kim H, Lee D-K, Sung S. Effect of urban green spaces and flooded area type on flooding probability. Sustainability 2016;8(2):134.
- [47] Klaassen P. Financial asset-pricing theory and stochastic programming models for asset/liability management: a synthesis. Manag Sci 1998;44(1):31–48.
- [48] Liu J, Sample DJ, Bell C, Guan Y. Review and research needs of bioretention used for the treatment of urban stormwater. Water (Basel) 2014;6(4):1069-99.
- [49] Liu W, Chen W, Peng C. Assessing the effectiveness of green infrastructures on urban flooding reduction: a community scale study. Ecol Modell 2014;291:6-14.
- [50] Liu W, Chen W, Peng C. Influences of setting sizes and combination of green infrastructures on community's stormwater runoff reduction. Ecol Modell 2015;318:236-44.
- [51] Loáiciga HA, Sadeghi KM, Shivers S, Kharaghani S. Stormwater control measures: optimization methods for sizing and selection. J Water Resour Plann Manag 2015:141(9):04015006.
- [52] Marti K. Stochastic optimization methods applications in engineering and operations research. Springer Berlin; 2016.
- [53] McCutcheon M, Wride D. Shades of green: using SWMM lid controls to simulate green infrastructure. J Water Manag Model 2013;R246-15:289-301.
- [54] McDonald RI, Green P, Balk D, Fekete BM, Revenga C, Todd M, et al. Urban growth, climate change, and freshwater availability. Proc Natl Acad Sci 2011;108(15):6312–17. [55] Meerow S, Newell JP. Spatial planning for multifunctional green infrastructure: growing resilience in detroit. Landsc Urban Plan 2017;159:62–75.
- [56] Moore TL, Gulliver JS, Stack L, Simpson MH. Stormwater management and climate change: vulnerability and capacity for adaptation in urban and suburban contexts. Clim Change 2016;138(3-4):491-504.
- [57] Obropta CC, Del Monaco N. Reducing directly connected impervious areas with green stormwater infrastructure. J Sustain Water Built Environ 2017;4(1):05017004. [58] City of Knoxville-Stormwater Engineering Division; 2018. [Last accessed on June 22, 2018]. http://knoxvilletn.gov/government/city_departments_offices/engineering/ stormwater engineering division
- [59] Oliver JE. Monthly precipitation distribution: a comparative index. Prof Geogr 1980;32(3):300-9.
- [60] Preston BL. Local path dependence of us socioeconomic exposure to climate extremes and the vulnerability commitment. Global Environ Change 2013;23(4):719–32.
- [61] Ramshani M, Khojandi A, Li X, Omitaomu OA. Optimal planning of the joint placement of photovoltaic panels and green roofs under climate change uncertainty; 2018. doi:10.1016/j.omega.2018.10.016.
- Rosa DJ, Clausen JC, Dietz ME. Calibration and verification of SWMM for low impact development. JAWRA J Am Water Resour Assoc 2015;51(3):746-57.
- [63] Rossman LA. Storm water management model user's manual, version 5.1. National Risk Management Research Laboratory, Office of Research and Development, US Environmental Protection Agency Cincinnati; 2015.
- Rouse DC, Bunster-Ossa IF. Green infrastructure: a landscape approach. Chicago: APA Planners Press; 2013. 571
- Shuster W, Dadio S. Soils investigation for infiltration-based green infras- tructure for sewershed management (Omaha NE). United States Environmental Protection Agency; 2014.
- [66] Snyder LV. Facility location under uncertainty: a review. IIE Trans 2006;38(7):547-64.

28

- [67] Soyster AL. Convex programming with set-inclusive constraints and applications to inexact linear programming. Oper Res 1973;21(5):1154-7.
- [68] Strassler E, Pritts J, Strellec K. Preliminary data summary of urban storm water best management practices. United States Environmental Protection Agency, Office of Water; 1999
- Traver RG, Ebrahimian A. Dynamic design of green stormwater infrastructure. Front Environ Sci Eng 2017;11(4):15.
- [70] Tsihrintzis VA, Hamid R. Modeling and management of urban stormwater runoff quality: a review. Water Resour Manag 1997;11(2):136-64.
- Tsihrintzis VA, Hamid R. Runoff quality prediction from small urban catchments using SWMM. Hydrol Process 1998;12(2):311-29.
- [72] U.S. Department of Labor, Bureau of Labor Statistics. CPI inflation calculator, [Last accessed on July 31, 2018]. https://www.bls.gov/data/inflation_calculator.htm.
- [73] World Health Organization (WHO). Global health observatory: Urban population growth; 2014. [Last accessed on January 28, 2016]. http://www.who.int/gho/urban_ health/situation_trends/.
- Zheng QP, Wang J, Liu AL. Stochastic optimization for unit commitment a review. IEEE Trans Power Syst 2015;30(4):1913-24.

Please cite this article as: M. Barah, A. Khojandi and X. Li et al., Optimizing green infrastructure placement under precipitation uncertainty, Omega, https://doi.org/10.1016/j.omega.2020.102196